2-25-2022

Identification of kidney injury released circulating osteopontin as causal agent of respiratory failure

Fatima Zohra Khamissi
Washington University School of Medicine in St. Louis

Liang Ning
Washington University School of Medicine in St. Louis

Eirini Kefaloyianni
Washington University School of Medicine in St. Louis

Hao Dun
Washington University School of Medicine in St. Louis

Akshayakeerthi Arthanarisami
Washington University School of Medicine in St. Louis

See next page for additional authors

HEALTH AND MEDICINE

Identification of kidney injury–released circulating osteopontin as causal agent of respiratory failure

Fatima Zohra Khamissi†, Liang Ning†, Eirini Kefaloyianni, Hao Dun, Akshayakeerthi Arthanarisami, Amy Keller, Jeffrey J. Atkinson, Wenjun Li, Brian Wong, Sabine Dietmann, Kory Lavine, Daniel Kreisel, Andreas Herrlich*

Tissue injury can drive secondary organ injury; however, mechanisms and mediators are not well understood. To identify interorgan cross-talk mediators, we used acute kidney injury (AKI)–induced acute lung injury (ALI) as a clinically important example. Using kidney and lung single-cell RNA sequencing after AKI in mice followed by ligand-receptor pairing analysis across organs, kidney ligands to lung receptors, we identify kidney-released circulating osteopontin (OPN) as a novel AKI-ALI mediator. OPN release from kidney tubule cells triggered lung endothelial leakage, inflammation, and respiratory failure. Pharmacological or genetic OPN inhibition prevented AKI-ALI. Transplantation of ischemic *wt* kidneys caused AKI-ALI, but not of ischemic OPN–global knockout kidneys, identifying kidney-released OPN as necessary interorgan signal to cause AKI-ALI. We show that OPN serum levels are elevated in patients with AKI and correlate with kidney injury. Our results demonstrate feasibility of using ligand-receptor analysis across organs to identify interorgan cross-talk mediators and may have important therapeutic implications in human AKI-ALI and multiorgan failure.

INTRODUCTION

Homeostasis in multicellular organisms and the response to its disturbance by injury is coordinated by cell-cell communication aimed at maintaining and reestablishing homeostasis (*1*–*3*). Studies on cellular functions in health and disease to date mostly focus on understanding cell-cell communication and its mediators within a given organ or diseased tissue (*4*). However, mediators of interorgan cross-talk between cells in different organs or tissues that drive multiorgan failure in complex diseases with high mortality and their cellular sources and target cells are largely unknown. Clinically important examples of this interorgan cross-talk include acute kidney injury (AKI)–induced acute lung injury (ALI) with respiratory failure (*5*, *6*), ALI, or its most severe form—acute respiratory distress syndrome (ARDS)—followed by AKI (*7*, *8*), or lung transplant–induced AKI (*9*).

We investigated interorgan cross-talk using the example AKI-ALI. AKI is a common problem in the human population and develops in 2 to 5% of patients during hospitalization, in 50% of intensive care unit patients, and in about 20% of kidney transplant patients within the first 6 months after transplantation (*9*). Irrespective of its cause, AKI alone has a 15 to 30% mortality, which rises to 60 to 80% when AKI induces remote secondary organ complications (multiorgan failure), particularly AKI-ALI (*5*, *6*, *10*). Molecular mechanisms and mediators of AKI-ALI are not yet well understood [reviewed in (*5*, *6*, *11*, *12*)]. Candidate AKI-ALI mediators were largely derived from global gene knockout (KO) studies or from the use of systemic interventions. These studies implicated interleukin-6 (IL6) (*13*, *14*) and tumor necrosis factor (TNF) (*15*), as well as IL10 released from splenic CD4 T cells (*16*), the alarmin high mobility group box-1 (*13*), and $CD8^+$ T cells (*14*) as putative mediators. For IL6 or TNF, as examples, it is known that AKI up-regulates their expression in the kidney, and elevated serum levels of IL6 and TNF protein after AKI were generally interpreted to result from release of these mediators by the injured kidney. However, AKI-ALI mediator expression has also been reported in extrarenal organs, such as IL6 expression in the liver, spleen, or lung (*15*, *16*), but cell type–specific KOs (kidney or other) of reported AKI-ALI mediators have not been tested in AKI-ALI models. Thus, it has not been conclusively shown that only or mainly the kidney serves as a source of these mediators after kidney injury. Furthermore, which lung cell types or immune cells are targeted by these mediators is largely unknown, except for a possible role of the TNF receptor TNFR1 in apoptosis of lung endothelial cells during AKI-ALI (*17*). Tissue-specific immune cell responses, in particular, of tissue resident or recruited macrophages, in the lung, heart, brain, liver, or kidney in response to myocardial infarction, stroke, or sepsis have been described (*18*). These immune cells might represent mediator targets, but interorgan signals that drive these responses or target immune cells are still largely unknown.

Hormones, growth factors, chemokines, cytokines, neurotransmitters, and other secreted proteins (in the following referred to as ligands) act in cell-cell communication in an autocrine/paracrine fashion locally but may have distant endocrine effects if released into the circulation. These ligands could be relevant for interorgan cross-talk, such as in the case of IL6 and TNF. We therefore chose to concentrate first on soluble ligands expressed in the kidney with the idea that these and the responding receptors expressed in lung cells will lead us to identify relevant causal mediators of interorgan communication. Ligand-induced cognate receptor activation in receiving cells generally results in altered gene expression and phenotypic changes. To date, ligand-receptor (L-R) pairing analysis using bulk or single-cell or single-nucleus RNA sequencing (scRNAseq or snRNA-seq) gene expression datasets has been used to infer cell-cell communication within a local tissue or organ (*1*, *4*). Here, we present, to our knowledge, the first L-R pairing analysis across different organs to successfully determine a mediator of interorgan cross-talk in multiorgan failure in vivo. Our studies identify kidney tubule

Washington University School in St. Louis School of Medicine, 660 S Euclid Avenue, St. Louis, MO 63110, USA.
*Corresponding author. Email: aherrlich@wustl.edu
†These authors contributed equally to this work.

cell–released circulating osteopontin (OPN) as a key causal mediator of AKI-induced remote ALI with respiratory failure (AKI-ALI).

RESULTS

Ischemic AKI causes severe ALI

Aiming at identifying communication between an injured tissue and other organs, we established a model of multiorgan failure. We chose to injure the kidney and study remote effects on the lung. We subjected C57BL/6 mice to bilateral renal ischemia-reperfusion injury (IRI) and analyzed remote ALI (AKI-ALI) (Fig. 1A, experimental scheme). Kidney injury caused highly elevated blood urea nitrogen (BUN) levels on day 1 after AKI, indicating severe kidney failure, with slow improvement by about 50% over days 3 to 5 (Fig. 1B). Consistent with this, serum creatinine was significantly elevated on day 1 and remained elevated at lower levels over days 3 to 5 (Fig. 1C). Severe injury to lungs and inflammation (AKI-ALI) followed with the same kinetics, as determined by expansion of interstitial spaces, increased cellularity and interstitial edema (Fig. 1D). Alveolar wall thickness increased over sham levels by 75% on day 1, signaling impediment of oxygenation (Fig. 1E). Neutrophils and interstitial macrophages (IMs) accumulated in the lung, peaked on day 1 after AKI, and were still significantly elevated by day 5. IMs that accumulated in lungs after AKI are small and $CD68^{low}$. Alveolar macrophages ($CD68^{high}$) did not change in numbers (Fig. 1F). We confirmed these results by mass cytometry [cytometry by time of flight (CyTOF)] of lung single-cell preparations from sham and AKI mice (Fig. 1G). Analysis of lung bronchoalveolar lavage (BAL) fluid on day 1 after AKI as compared to BAL fluid from sham controls showed significantly increased total protein and albumin concentration (Fig. 1H), as well as increased total immune cells and neutrophils; alveolar macrophage numbers were similar to sham control (Fig. 1I). These BAL findings are consistent with substantial AKI-ALI. The functional consequence of these changes was a significant impairment in oxygen exchange on day 1 after AKI (Fig. 1J). Our mouse data thus closely resemble what can be observed in patients with multiorgan failure after AKI (*5*, *6*, *8*).

To exclude that the observed AKI-ALI phenotype is simply the result of accumulation of toxic waste products or failure to excrete an existing potentially detrimental molecule because of lack of glomerular filtration, we examined mice for AKI-ALI on day 1 after simple bilateral nephrectomy, without reperfusion injury. Sham-operated mice or animals that underwent bilateral nephrectomies showed no differences in terms of lung interstitial spaces and cellularity (Fig. 1K), alveolar wall thickness (Fig. 1L), or lung immune cell numbers as assessed by CyTOF on day 1 after nephrectomy (Fig. 1M). These findings indicate that AKI-ALI in our model does not develop simply because of a failure to excrete a potentially detrimental molecule.

scRNAseq of kidney and lung in setting of AKI-ALI

As an entrance into identifying relevant cellular changes after AKI, we analyzed cellular gene expression profiles by scRNAseq of kidneys and lungs isolated on day 1 after sham operation or bilateral renal IRI-induced AKI (Fig. 2A, experimental scheme). Serum BUN levels were significantly elevated in injured mice on day 1 after AKI (Fig. 2B), indicating severe AKI. Analysis of scRNAseq gene expression profiles revealed the presence of all known nonimmune and immune cell types of the kidney and lung. Seurat objects that combine the data for sham and injury, as well as dotplots identifying standard marker genes used to identify cell types (*19*, *20*), for either kidney (Fig. 2, C and D) or lung (Fig. 2, E and F), are shown. To monitor specific changes between sham and injury, we replotted our scRNAseq data separately for sham and injury of the kidney or lung. On the basis of number of cells captured in each population (Seurat cluster), the injured kidney in comparison to sham showed easily detectable and expected dynamics in the immune cell compartment, with strong enrichment of neutrophils and monocytes in the injured sample (Fig. 2G). Similar but somewhat more subtle changes were detected in the same immune cells in the remotely injured lung. We detected a strong increase in the number of neutrophils and a small increase in monocytes in remotely injured lung tissue (Fig. 2H). Changes in lung IM numbers between sham and injury were less appreciable at this level of our scRNAseq analysis, although we detected them in large numbers (Fig. 2, G and H).

L-R pairing analysis across organs, linking ligands expressed in the kidney to receptors expressed in the lung

To infer possible cell-cell communication events between kidneys and lungs, we used the machine learning algorithm CellPhoneDB (*21*) to perform computational L-R pairing analysis across organs, with ligands located in the kidney and their cognate receptors in the lung (Fig. 3A). The CellPhoneDB L-R interaction database used here is unique in that, beyond classical ligand and receptor interactions, it also considers other interaction partners that may participate in signaling, such as co-receptors or other receptor-associated proteins. We considered only L-R interactions with the ligand expressed in a kidney cell type and its cognate receptor expressed in a lung cell type. Notably, CellPhoneDB calculates an empirical *P* value, with higher *P* values indicating higher predicted significance of the L-R pairing.

We divided our analysis into L-R pairings from nonimmune cells or immune cell types in the kidney to nonimmune cells or immune cell types in the lung, either at baseline (sham) or after injury (AKI kidney or AKI-ALI lung). The top scoring L-R pairing detected at baseline and after injury was tubule cell-expressed OPN [or secreted phosphoprotein-1 (SPP1)] pairing with its receptor CD44 in lung nonimmune and immune cell types. The significance of these predicted interactions was $P > 2.5$ at baseline, which significantly increased to $P > 4.5$ after injury. At baseline, distal tubule cells represented the main source of OPN, but, by day 1 after AKI, proximal tubule cells were also predicted to significantly participate in OPN:CD44 signaling (Fig. 3, B and C, panels 1 and 2). CD44 has several other ligands, some of which were also detected in the L-R pairing analysis, such as hepatocyte growth factor (HGF):CD44 or fibroblast growth factor 2 (FGF2):CD44, but these pairings were limited to kidney immune to lung immune cell pairings and of low to moderate significance that did not change with injury (fig. S1A, panels 1 and 2). For kidney immune cells, the top scoring L-R pairings, however, with low difference in significance between sham and injured samples ($P > 2.5 \rightarrow 3$) included (i) kidney neutrophil IL1β connecting to β2-adrenergic receptor (IL1b:Adrb2) in lung immune or stromal cells and (ii) kidney T cell chemokine ligand 5 (CCL5) connecting to CCR1-5/atypical chemokine receptor 4 (Ackr4) receptors in lung immune or nonimmune cells (fig. S1, A and B, panels 1 and 2). The significance of the IL1b:Adrb2 pairing is unclear, as this pairing is predicted by CellPhoneDB on the basis of protein-protein interaction data curated from various experimental approaches (*22*, *23*), but it is not known whether this interaction produces a cellular signal.

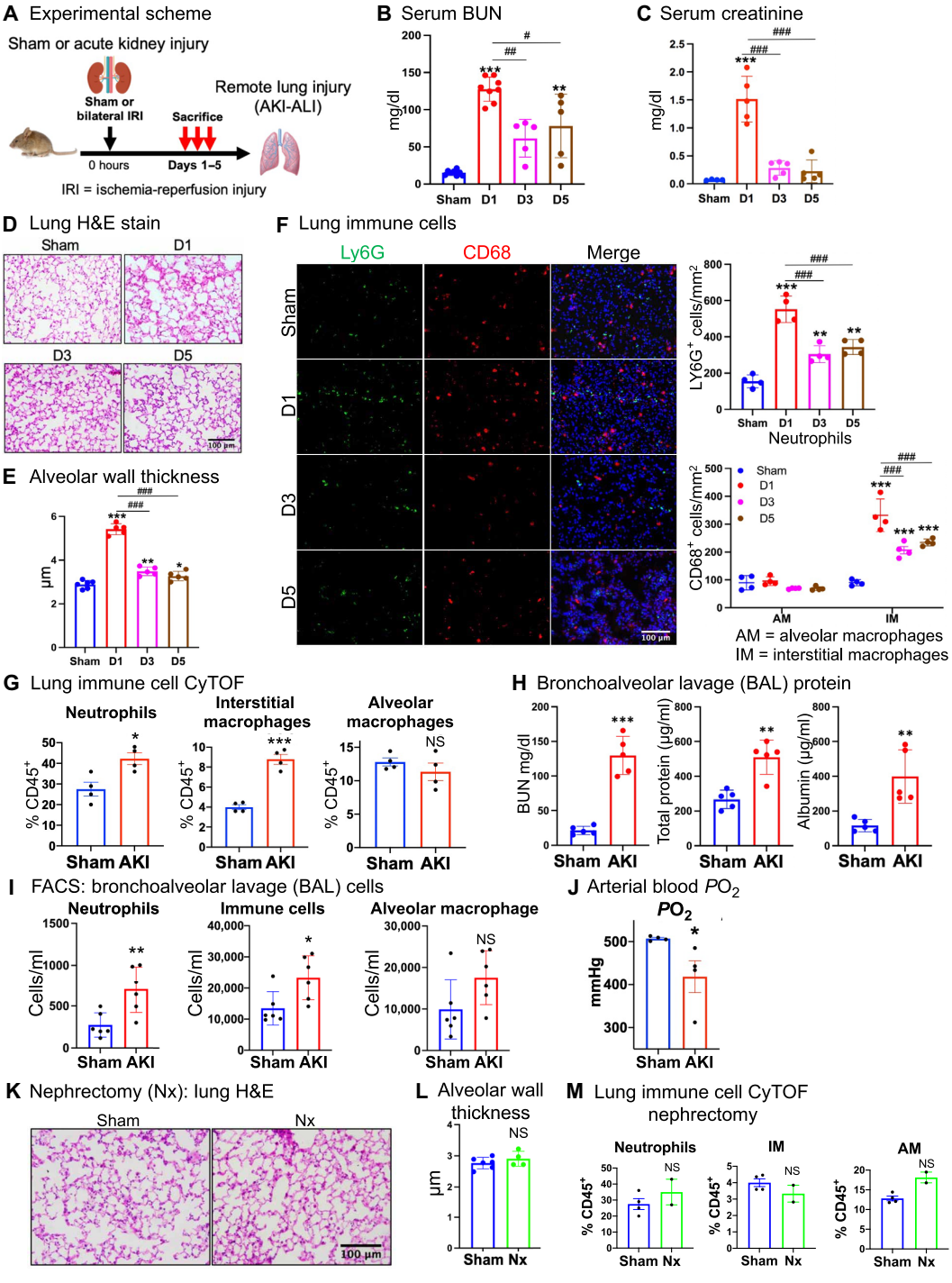

Fig. 1. Ischemic AKI causes severe ALI. (**A**) Experimental scheme: AKI ➔ AKI-ALI model sham, days 1, 3, and 5 after AKI. (**B**) Serum BUN values after sham or AKI, days 1 to 5. (**C**) Serum creatinine values after sham or AKI, days 1 to 5. (**D**) Hematoxylin and eosin (H&E) stain lung after sham or AKI, days 1 to 5. (**E**) Alveolar wall thickness measurements after sham or AKI, days 1 to 5. (**F**) Lung neutrophils (Ly6G$^+$, green), alveolar macrophages (AMs) (CD68^{high}, large, red), and IMs (CD68^{low}, small, red) and quantification after sham or AKI, days 1 to 5. 4′,6-diamidino-2-phenylindole (DAPI) stain (blue) was used to visualize nuclei. (**G**) CyTOF: lung neutrophils (CD45$^+$ and Ly6G$^+$), alveolar macrophages (CD45$^+$, CD68^{high}, and Siglec-F$^+$), and lung IMs (CD45$^+$, CD68^{low}, and Siglec-F$^-$), day 1. (**H**) BAL protein/albumin analysis: serum BUN elevations and BAL fluid protein/albumin after sham or AKI, day 1. Total protein was detected by the Pierce BCA Protein Assay. Albumin was detected by enzyme-linked immunosorbent assay (ELISA). (**I**) BAL immune cell analysis: Total immune cells, macrophages, and neutrophils were detected by fluorescence-activated cell sorting (FACS). (**J**) Arterial blood oxygen partial pressure (PO_2) after sham or AKI, day 1. (**K**) Lung hematoxylin and eosin after sham or nephrectomy (Nx), day 1. (**L**) Alveolar wall thickness after sham or nephrectomy, day 1. (**M**) CyTOF: Lung neutrophils (CD45$^+$ and Ly6G$^+$), alveolar macrophages (CD45$^+$, CD68^{high}, and Siglec-F$^-$), and lung IMs (CD45$^+$, CD68^{low}, and Siglec-F$^-$) were quantified after sham or nephrectomy, day 1. $n = 4$ to 8 animals per measurement. *$P < 0.05$, **$P < 0.01$, ***$P < 0.001$, #$P < 0.05$, ##$P < 0.01$, and ###$P < 0.001$. NS, not significant.

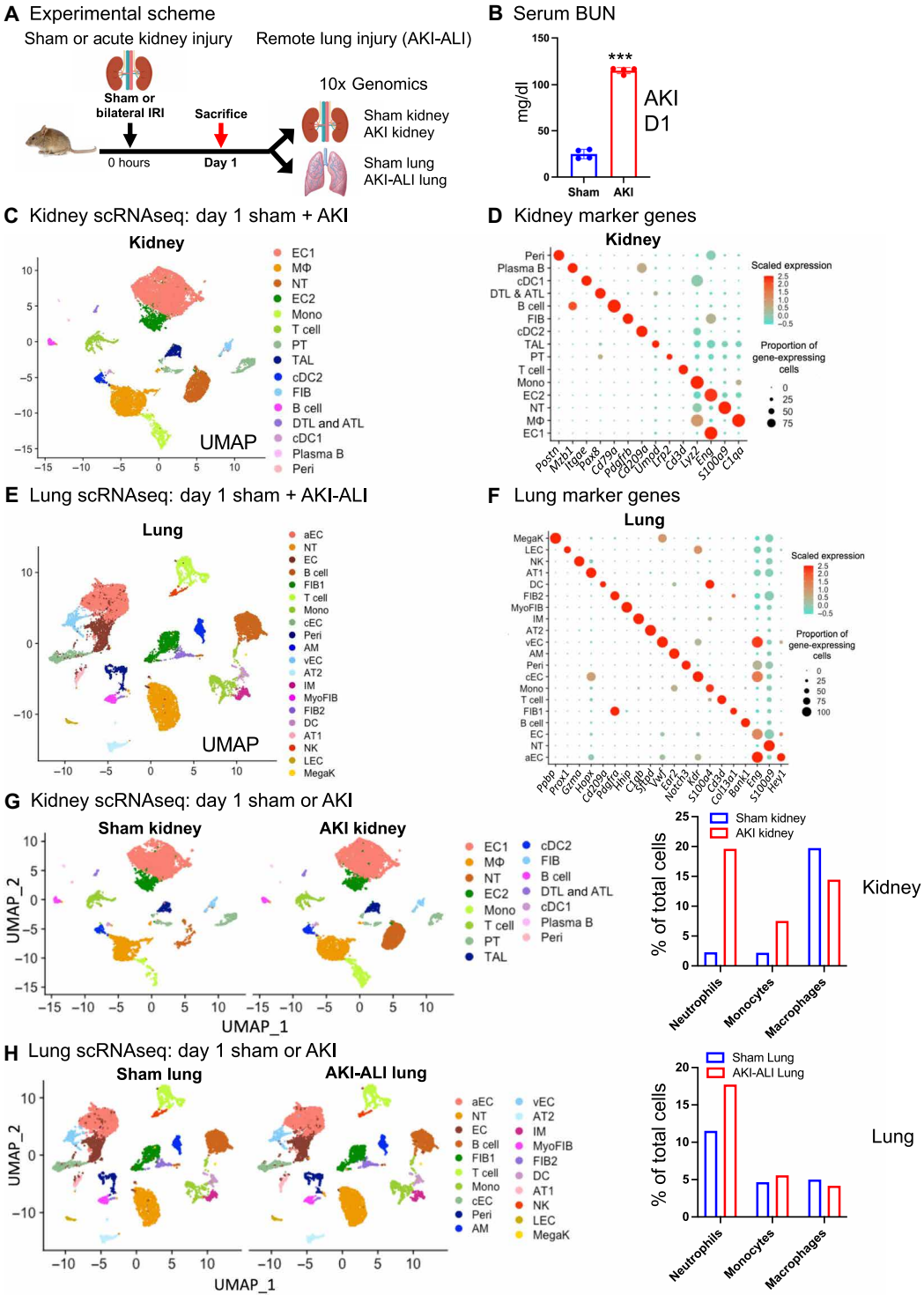

Fig. 2. scRNAseq of kidney and lung in setting of AKI-ALI. (**A**) Experimental scheme: scRNAseq 10x Genomics of kidney and lung day 1 after sham or AKI. (**B**) Serum BUN values after sham or AKI, day 1. (**C**) Seurat object: combined kidney sham and AKI, day 1. (**D**) Marker genes used for definition of kidney cell types. (**E**) Seurat object: combined lung sham and AKI-ALI lung, day 1. (**F**) Marker genes used for definition of lung cell types. (**G**) Seurat objects: sham kidney versus AKI kidney, day 1, quantification of neutrophils, monocytes, and macrophages in sham or AKI samples expressed as the percentage of total cells detected by Seurat. (**H**) Seurat objects: sham lung versus AKI-ALI lung, day 1, quantification of neutrophils, monocytes, and macrophages in sham or AKI samples expressed as the percentage of total cells detected by Seurat. Cell types: epithelial: AT1/2, type 1/2 lung epithelial cell; PT, proximal tubule; TAL, thick ascending limb; DTL, descending-type thin limb; ATL, ascending-type thin limb. Endothelial: EC, endothelial cell (a, arterial; v, venous; c, capillary). Stromal: FIB, fibroblast; PERI, pericyte. Immune cells: NT, neutrophil; DC, dendritic cell; MΦ, macrophage; AM; IM; Mono, monocyte; MegaK, megakaryocyte; Plasma B, plasma B cell; B cell; T cell. $n = 4$ animals per measurement. ***$P < 0.001$.

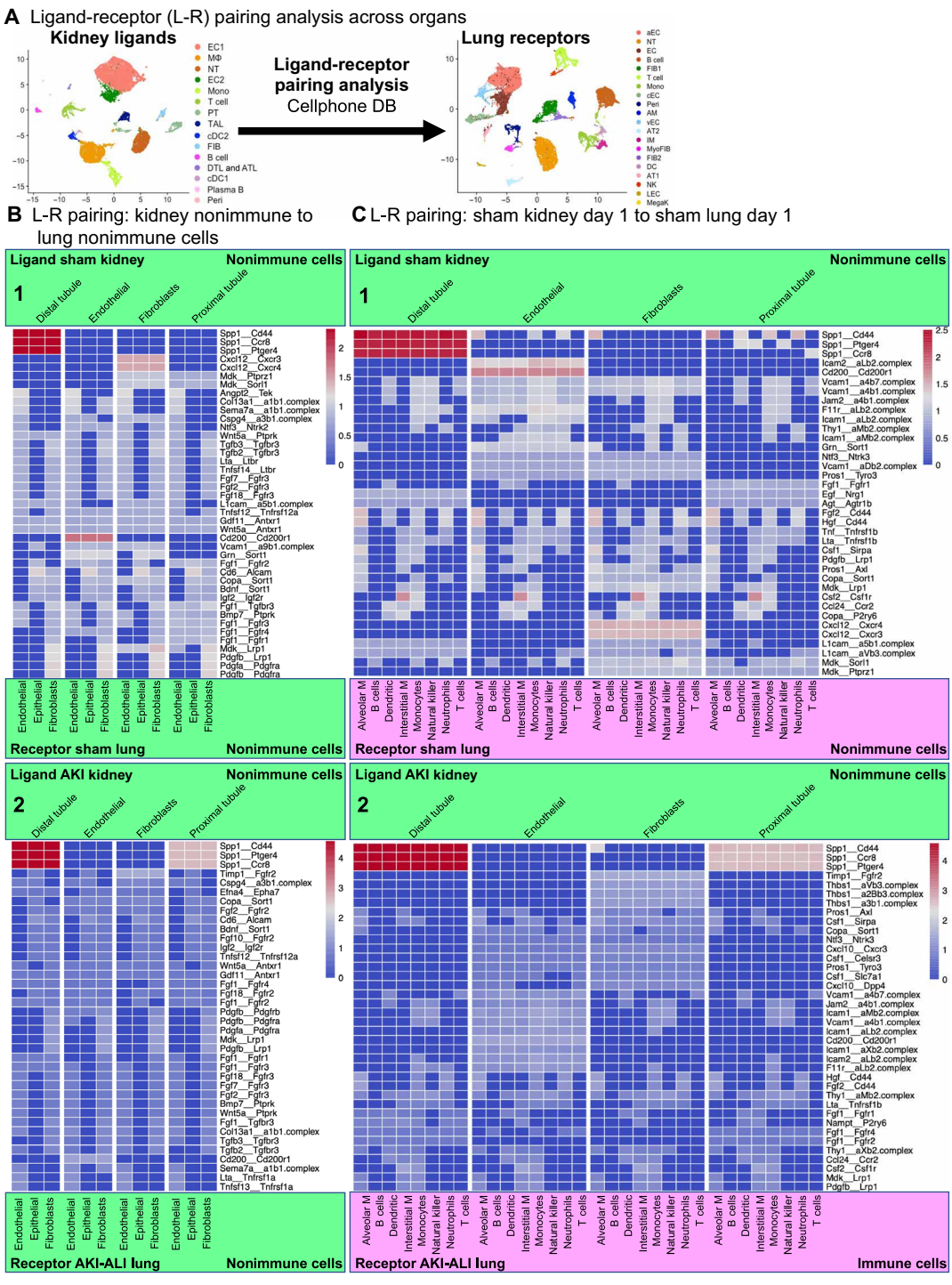

Fig. 3. L-R pairing analysis across organs, linking ligands expressed in the kidney to receptors expressed in the lung. (**A**) Experimental scheme: design of L-R pairing analysis, kidney ligands paired to lung receptors using kidney and lung scRNAseq data and CellPhoneDB analysis. (**B**) L-R pairing analysis kidney nonimmune cells to lung nonimmune cells for day 1 after sham (panel 1) or AKI (panel 2). *P* values shown are empirical *P* values calculated by CellPhoneDB, and higher values indicate higher L-R pairing significance.

Whether T cell released CCL5 or CCL5, in general, is involved in AKI-ALI is unknown.

We validated our CellPhoneDB analysis using two approaches. First, we used a previously published snRNAseq dataset that assessed kidney gene expression at early time points after AKI for our L-R pairing analysis (*19*). We linked their kidney snRNAseq dataset of 4 and 12 hours after AKI to our scRNAseq data of the remotely injured AKI-ALI lung at day 1 after AKI. L-R pairing analysis identified OPN:CD44 as a top hit. Kidney distal tubule OPN pairing with CD44 receptor in lung immune and nonimmune cell types

showed high significance at 4 hours after AKI. At 12 hours after AKI, OPN derived from several kidney cell types including distal tubule cells, endothelial cells, fibroblasts, macrophages, and T cells pairing with CD44 in lung immune or nonimmune cells represented the top scoring L-R pairing (fig. S2, A and B). Second, we used a list of all secreted proteins identified in UniProt and added a hand-curated list of additional secreted or metalloprotease released proteins of interest and assessed their average expression in all cell types of our AKI kidney scRNAseq dataset. In this analysis, OPN also emerged as the top distal tubule secreted molecule after AKI, and none of the secreted proteins, which were not included in CellPhoneDB, showed a comparable increase.

OPN (SPP1), initially identified as a regulator of bone biomineralization and remodeling, is an immunoregulatory molecule expressed in a variety of cells, including stromal, epithelial, and immune cells (*24*–*28*). OPN is strongly chemotactic for immune cells, in particular, for neutrophils and macrophages and enhances T helper 1 inflammation (*29*, *30*). Taking these immunoregulatory features of OPN and our L-R pairing analysis and in silico validation into account, we hypothesized that OPN might be a good candidate AKI-ALI mediator to study in our AKI-ALI model.

OPN is up-regulated in kidneys but not in lungs during AKI-ALI

To understand the relationship between OPN and the development of AKI-ALI, we assessed expression patterns of OPN mRNA and OPN protein serum levels during the course of AKI. On the basis of our scRNAseq data, OPN mRNA is already expressed at significant levels in distal tubule and to a lesser degree in proximal tubule cells of sham kidneys (Fig. 4A, top). On day 1 after AKI, OPN expression was not only most significantly increased in both proximal and distal tubule cells but, now, also present at lower levels in other cell types such as endothelial cells, fibroblasts, neutrophils, macrophages, and T cells (Fig. 4A, bottom). This suggests that tubule-released OPN could potentially act in the induction phase of AKI-ALI and that, at later stages, various cellular OPN sources, including immune cells, might contribute to elevated OPN serum levels. We validated these findings by comparing our scRNAseq data with previously published snRNAseq AKI data (*19*). Similar to our dataset, OPN mRNA expression in sham kidneys was present in both proximal tubule cells (PTC and new PTC) and distal tubule cells [CNT (connecting tubule), descending-type thin limb–ascending-type thin limb (DTL-ATL), DCT (Distal Convoluted Tubule), and Uro (Urothelium)]. By 4 hours after AKI, OPN mRNA expression began to increase significantly in several cell types, and by 12 hours, OPN mRNA expression was very high in proximal and distal tubules, endothelial cells, fibroblasts, neutrophils, macrophages, and T cells, similar to our dataset on day 1 after AKI. OPN expression remained elevated for several weeks in distal tubular compartments (Fig. 4B). In contrast to the kidney, OPN expression in sham lung was only present in moderate levels in pericytes and, to a lesser degree, in resident alveolar macrophages. AKI injury did not change the overall low OPN expression levels detected by scRNAseq in the lung on day 1 after AKI (Fig. 4C, top and bottom), suggesting that the kidney but not the lung represents a substantial source of OPN after AKI. To better understand dynamic changes in our model, we performed additional AKI-ALI experiments, evaluating earlier time points. We subjected C57BL/6 mice to AKI and euthanized them 1, 2, 4, 6, and 12 hours later (Fig. 4D, experimental scheme). In Figs. 4 and 5, we are also incorporating AKI-ALI data from day 1, 3, or 5 after AKI derived from Fig. 1 for ease of viewing. Serum BUN and serum creatinine levels were already significantly elevated 1 hour after AKI (Fig. 4, E and F), and serum kidney injury molecule-1 (KIM-1; a sensitive marker of kidney injury) was elevated at 12 hours (Fig. 4G), indicating substantial kidney injury. Kidney OPN expression was already significantly elevated 2 to 4 hours after AKI, reached a peak by 12 hours, and remained elevated until at least day 5. Lung OPN expression, however, remained virtually undetectable or very low over the same time (Fig. 4H). Serum OPN protein levels closely followed changes in kidney OPN mRNA expression (Fig. 4I). The early rise in OPN serum levels is likely enabled by the existing baseline expression of OPN in the sham kidney (Fig. 4, A and B). Elevated OPN levels in AKI-injured mice correlated with the degree of kidney injury (BUN/OPN) (Fig. 4J).

Serum OPN protein levels have been studied as a biomarker of severity of disease in patients with multiorgan failure, often including AKI and ALI (*31*, *32*). Whether serum OPN levels are also elevated in patients with AKI before development of multiorgan failure is not known. We examined OPN serum levels in patients with AKI that did not have multiorgan failure and were not critically ill. Serum OPN levels were significantly elevated in patients with AKI, as compared to healthy controls or patients with chronic kidney disease (CKD) (Fig. 4K) and positively correlated with reduced kidney function as determined by serum creatinine measurements (Fig. 4L). These findings suggest that AKI in humans could result in release of substantial amounts of OPN into the circulation and raise the possibility that circulating OPN may promote damage at remote sites also in humans.

We hypothesized that for OPN to act on lung and cause AKI-ALI, it might need to gain access to the lung tissue compartment from the circulation. Alternatively, it could act on cells directly accessible from the circulation, such as endothelial cells or circulating immune cells. We thus examined whether OPN can gain access to lung tissue from the circulation in the setting of AKI in mice. We injected fluorescently labeled OPN after sham operation or after AKI at the time of reperfusion and euthanized animals 30 min or 1 hour after injection. We costained for nidogen, a marker of the extracellular matrix/interstitial space. Sham-operated animals did not accumulate any significant amount of fluorescently marked OPN in the lung within 1 hour of injection, whereas animals with AKI showed OPN accumulation in lung interstitium (thin arrows) and colocalization with lung cells (thick arrows) at 30 min or 1 hour after injection (fig. S4). Ly6G, CD68, and CD44 costains reveal that injected fluorescently marked OPN colocalizes with $CD68^+$ alveolar macrophages and IMs (which also show the highest staining for CD44) but not with Ly6G-positive neutrophils (Fig. 4M). Together, our results indicate that kidney rather than lung represents the source of circulating OPN protein after AKI and that circulating OPN can principally gain access to the lung early after AKI and thus might mediate the induction of remote lung injury. As predicted from the L-R pairing analysis in Fig. 3, CD44 in lung immune cells, particularly alveolar macrophages and IMs, may represent important targets of OPN released from the kidney. Access to the lung was marginal in sham-operated animals, leading us to the conclusion that another AKI-released factor must cooperate with OPN to allow OPN access to lung tissue.

AKI triggers lung endothelial barrier dysfunction and immune cell accumulation very early after injury

Consistent with the timing of elevated OPN serum levels after AKI, lungs already showed significant signs of injury with interstitial

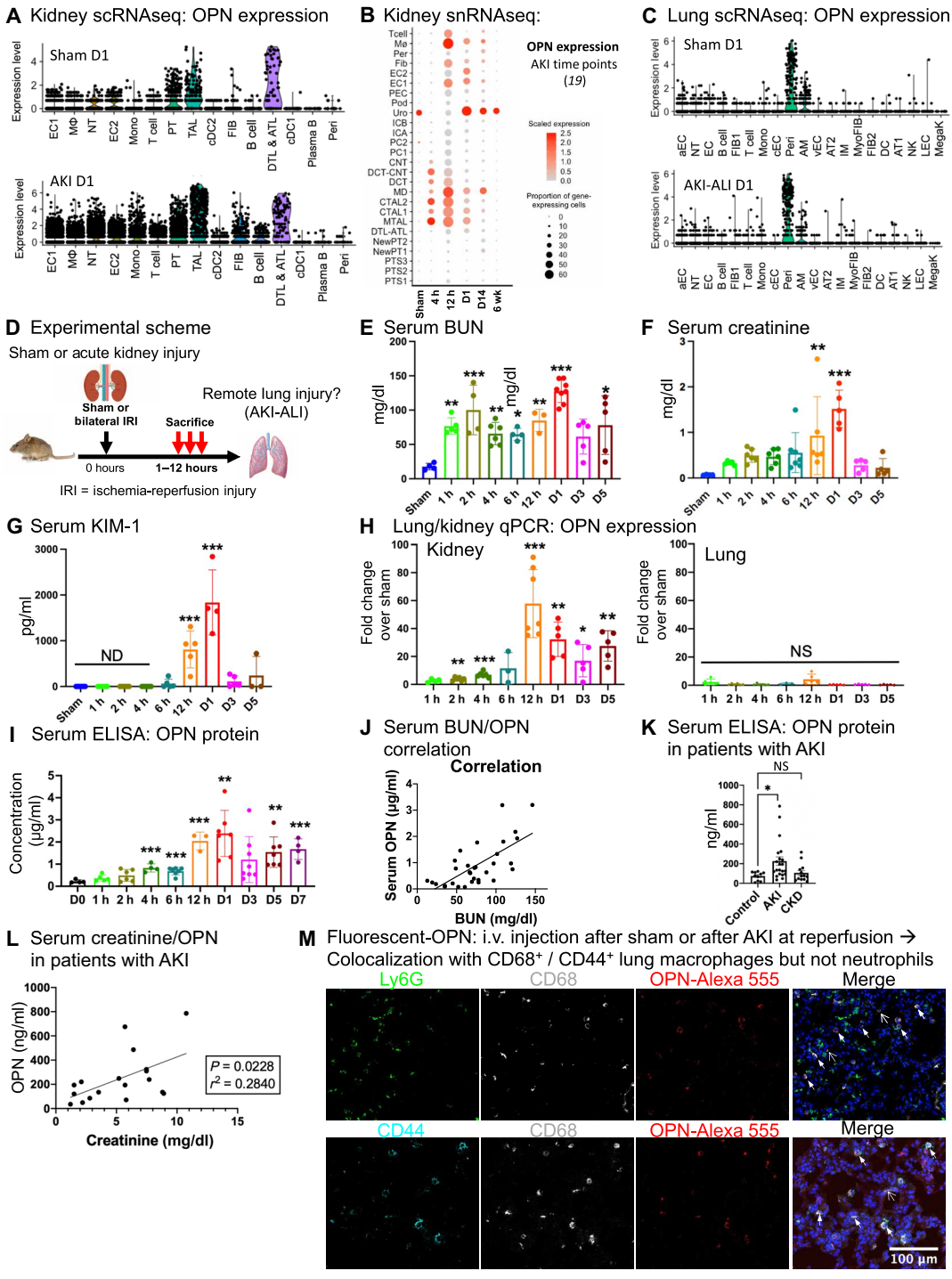

Fig. 4. OPN is up-regulated in kidneys but not lungs during AKI-ALI. (**A**) Kidney scRNAseq: OPN expression after sham (top) or AKI (bottom). (**B**) Kidney snRNAseq (*20*): OPN expression after sham or 4 hours, 12 hours, 2 days, 14 days, and 6 weeks after AKI. (**C**) Lung scRNAseq: OPN expression after sham (top) or AKI (bottom). (**D**) Experimental scheme: AKI ➔ AKI-ALI model. Sham, 1, 2, 4, and 12 hours after AKI. We integrated measurements from days 1, 3, and 5 after AKI (Fig. 1) in some panels of Fig. 4. (**E**) Serum BUN after sham or 1 to 12 hours and days 1, 3, and 5 after AKI. (**F**) Serum creatinine after sham or 1 to 12 hours and days 1, 3, and 5 after AKI. (**G**) Serum KIM-1 after sham or 1 to 12 hours and days 1, 3, and 5 after AKI. (**H**) Kidney + lung quantitative polymerase chain reaction (qPCR): OPN expression after sham or 1 to 12 hours and days 1, 3, and 5 after AKI. (**I**) Serum ELISA: OPN protein after sham or 1 to 12 hours and days 1, 3, and 5 after AKI. (**J**) Serum BUN/OPN correlation using BUN and OPN measurements across all time points. (**K**) Serum ELISA: human OPN protein levels in patients with AKI compared to healthy controls and patients with chronic kidney disease (CKD). (**L**) Correlation of OPN serum levels with serum creatinine concentration in patients with AKI. (**M**) Colocalization of OPN Alexa Fluor 555 (Alexa 555) with $CD68^+/CD44^+$ alveolar macrophages (fat arrows) and IMs (thin arrows) but not with $Ly6G^+$ neutrophils. Arrows show colocalization with CD68/CD44. $n = 3$ to 8 animals per measurement. $^*P < 0.05$, $^{**}P < 0.01$, and $^{***}P < 0.001$. ND, not detected; i.v., intravenous.

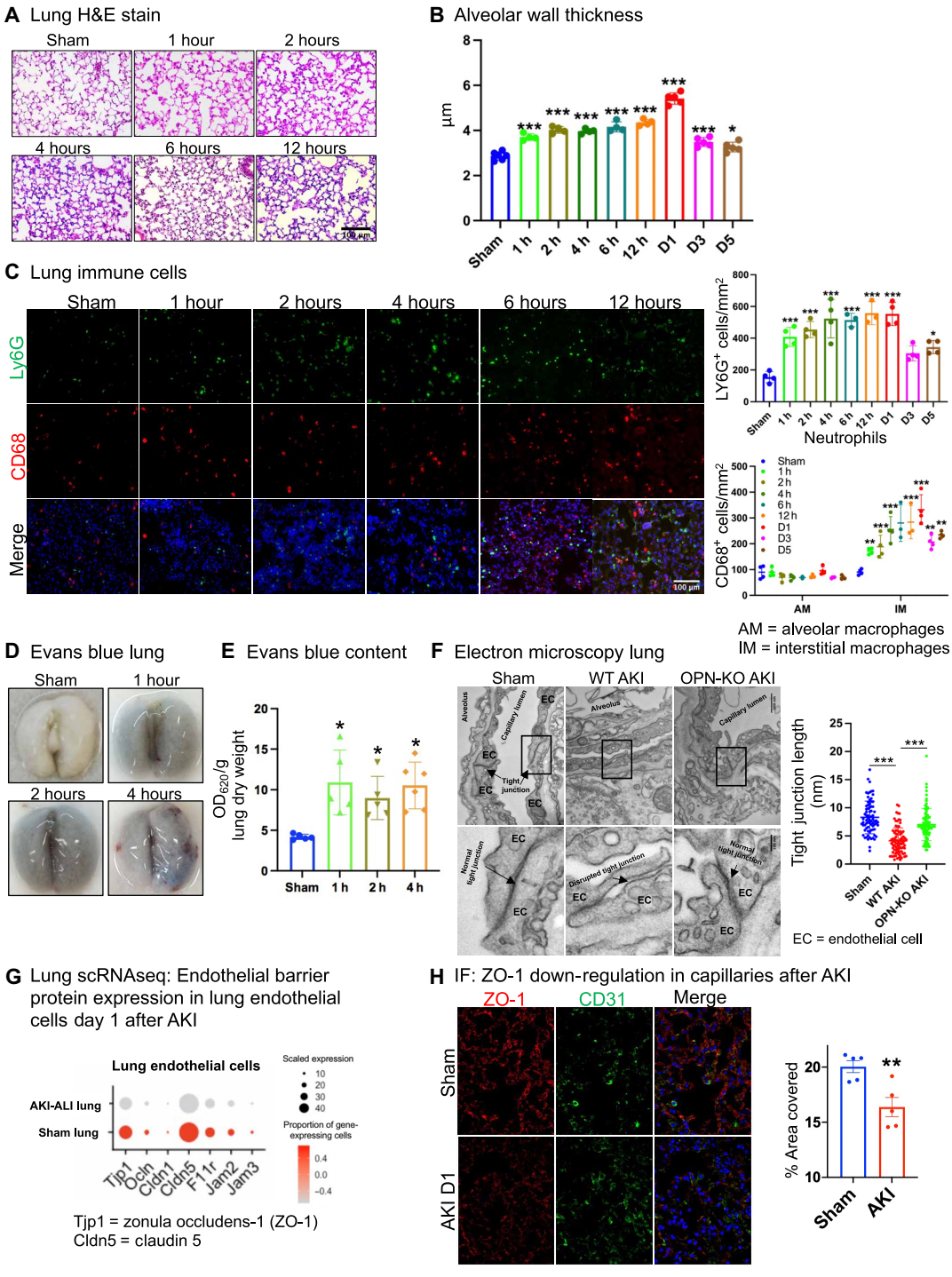

Fig. 5. AKI triggers lung endothelial barrier dysfunction and immune cell accumulation very early after AKI. (**A**) Lung hematoxylin and eosin stain after sham or 1 to 12 hours after AKI. (**B**) Alveolar wall thickness measurements after sham or 1 to 12 hours and days 1, 3, and 5 after AKI. (**C**) Lung neutrophils (Ly6G^{+}, green), alveolar macrophages (CD68^{high}, large, red), and IMs (CD68^{low}, small, red) and quantification after Sham or AKI days 1, 3, and 5 after AKI. DAPI stain (blue) was used to visualize nuclei. (**D**) Lung Evans blue leakage after sham or 1 to 4 hours after AKI. (**E**) Lung Evans blue quantification [optical density at 620 nm (OD_{620}) per gram of lung dry weight] after sham or 1 to 4 hours after AKI. (**F**) Lung electron microscopy and quantification of endothelial tight junction length (in nanometers) at day 1 in sham or day 1 after AKI in *wt* control or OPN–global KO mice. (**G**) Lung scRNAseq: expression of endothelial barrier proteins in lung endothelial cells day 1 after sham or AKI; Tjp1: zonula occludens-1 (ZO-1) and claudin-5 (Cdnl5). (**H**) Lung ZO-1 protein expression [immunofluorescence (IF)]: ZO-1 (red), CD31 (green, marking endothelial cells), DAPI (blue, marking nucleus), and quantification day 1 after sham or AKI. (**I**) Lung qPCR: ZO-1 expression day 1 after sham or AKI. $n = 3$ to 6animals per measurement. $^{*}P < 0.05$, $^{**}P < 0.01$, and $^{***}P < 0.001$.

expansion and increased cellularity by 1 hour after AKI, which worsened progressively over the subsequent 12 hours (Fig. 5A, also compare to Fig. 1D). Alveolar wall thickness increased significantly by 1 hour (>1.3-fold increase over sham), worsened progressively over the ensuing 12 hours (>1.5-fold increase over sham), and reached a peak at day 1 after AKI (>1.85-fold increase over sham) (Fig. 5B). Consistent with these findings, accumulation of neutrophils and macrophages showed a similar trend to the timeline of changes in kidney OPN mRNA expression and serum OPN levels (Fig. 5C).

Endothelial homeostasis is disrupted in ALI or its most severe form, ARDS, which often occurs in response to direct lung injury, such as by coronavirus disease 2019 (COVID-19) lung infection (*33*), or as a secondary organ complication of sepsis (*34*, *35*). Severe ALI/ARDS is characterized by diffuse endothelial injury, intense activation of the coagulation system, and increased capillary permeability (*33*, *36*). Increased vascular barrier permeability has also been reported in animal models of AKI (*13*, *37*, *38*). We thus set out to examine whether endothelial barrier disruption, a hallmark of lung injury, also occurs following AKI in our model. Vascular leakage, as evidenced by Evans blue dye uptake, was already detectable at a level twice as high as sham controls at 1 hour after AKI, which was maintained for at least 4 hours (Fig. 5, D and E). Electron microscopy also showed that, compared to sham controls, endothelial tight junctions in AKI-injured C57BL/6 animals were shortened in length or disrupted in day 1 AKI-ALI lungs. By contrast, AKI-injured OPN–global KO mice displayed normal endothelial tight junctions, comparable to sham-operated *wt* animals (Fig. 5F). We next assessed lung endothelial cells. Using our scRNAseq data, we found that the expression levels of two endothelial barrier proteins, zonula occludens-1 [ZO-1; *Tjp1* (tight junction protein 1)] and claudin-5 (*Cldn5*), were strongly down-regulated in AKI-ALI samples as compared to sham lungs (Fig. 5G). We validated our finding on the protein level for ZO-1. ZO-1 staining was heavily present in the capillary network of sham lung but severely diminished in the capillary network of the AKI-ALI lung. CD31 (green) was used as a costain to identify endothelial cells (Fig. 5H). Other cell types in the lung, particularly stromal cells, such as fibroblasts and lung epithelial cells (AT1/2), also expressed ZO-1 or Cldn5 at low levels, and these expression levels did not significantly change in the AKI-ALI lung. These results suggest that endothelial barrier dysfunction and vascular leakage represent early events in the induction of AKI-ALI remote lung injury in our model.

Pharmacological or genetic inhibition of OPN protects from ALI after AKI

To assess whether OPN is necessary for the development of AKI-ALI, we subjected C57BL/6 mice to bilateral IRI and injected the animals with either control immunoglobulin G (IgG) or anti-OPN neutralizing antibody. Analogous experiments were performed in OPN–global KO or *wt* mice without antibody treatments (Fig. 6A, experimental scheme). Anti-OPN antibody–treated mice or OPN–global KO mice experienced the same degree of kidney injury on day 1 as controls, as evidenced by comparable elevations in serum BUN and KIM-1 levels (Fig. 6, B and C). However, lung injury was significantly ameliorated after treatment with anti-OPN antibody and in OPN–global KO mice (Fig. 6, D and E). While anti-OPN antibody strongly reduced lung neutrophil and IM accumulation after AKI, OPN–global KO prevented it almost completely (Fig. 6F). Anti-OPN antibody–treated animals also showed strongly reduced vascular leakage and improved lung function as compared to controls on day 1 after AKI (Fig. 6, G to I). Together, our results identify circulating OPN as a critical and necessary regulator of lung endothelial barrier permeability, lung immune cell accumulation, and functional impairment in AKI-ALI.

Circulating OPN is sufficient to induce ALI after AKI

To determine whether OPN suffices to mediate AKI-ALI, we tested the effect of OPN injection in the context of mild AKI (reduced ischemia time), an experimental condition where AKI-ALI is not detectable at 6 hours after AKI (Fig. 7A, experimental scheme). As expected, serum OPN levels were significantly lower in mild AKI than severe AKI (Fig. 7B). Serum BUN levels were significantly elevated at 6 hours after mild AKI compared to sham controls but lower compared to severe AKI (Fig. 7C). Intravenous injection of OPN protein into mild AKI animals at the time of kidney reperfusion at quantities that would mimic serum concentrations at 6 hours after severe AKI (see Fig. 4I) triggered AKI-ALI that was now comparable to severe AKI-ALI (Fig. 7, E and F). We also performed OPN injections into uninjured mice but were unable to detect increases in alveolar wall thickness or inflammatory changes in the lung (fig. S3), suggesting that a second event or mediator induced by AKI is required for OPN to successfully induce AKI-ALI. Therefore, we conclude that OPN is sufficient to induce AKI-ALI only in the context of AKI.

Circulating OPN relevant for induction of AKI-ALI is released from the injured kidney

Up-regulated OPN expression and serum levels have been found in the context of a number of organ injuries (*31*, *32*, *39*–*45*), allowing for the possibility that OPN sources in the body other than the kidney might be relevant in AKI-ALI. Conversely, it has never been conclusively shown that a proposed AKI-ALI mediator is released directly from the injured kidney. To address this question, we performed kidney transplantation experiments, where we transplanted either ischemic *wt* kidneys or ischemic OPN–global KO kidneys into syngeneic C57BL/6 mice (Fig. 8A, experimental scheme). KIM-1 kidney mRNA expression and tubular injury scores document that transplanted OPN–global KO kidneys show kidney injury parameters comparable to those in transplanted *wt* kidneys (Fig. 8, B and C). Serum BUN and creatinine measurements would be unaffected in our transplantation model, given that two intact kidneys are present in the mouse as well. OPN serum levels were elevated above sham levels in mice that received *wt* kidneys but not in mice that were transplanted OPN-KO renal grafts. Notably, OPN serum levels are lower with only one injured transplant kidney, as compared to the bilateral IRI model, where two kidneys are injured (Fig. 8D; see also Fig. 4). Lung injury developed in mice that received *wt* kidneys but not in those that received OPN-KO kidney grafts (Fig. 8, E to I). These results conclusively identify the kidneys as the source of OPN during the development of ALI after AKI. Last, when ischemic *wt* kidneys are transplanted into OPN–global KO mice (Fig. 9A), the protection of the latter from developing AKI-ALI is reversed, and these mice develop AKI-ALI similar to *wt* mice transplanted with ischemic *wt* kidneys (Fig. 9B). Alveolar wall thickness increases (Fig. 9C), and infiltration of immune cells is now equal to the effect of *wt* kidney transplant into *wt* mice (Fig. 9D). OPN released from the transplanted *wt* kidney is detectable in the lung and colocalizes with $CD68^+$ and $CD44^+$ alveolar macrophages and IMs but not with $Ly6G^+$ neutrophils (Fig. 9E), identical to exogenously injected OPN

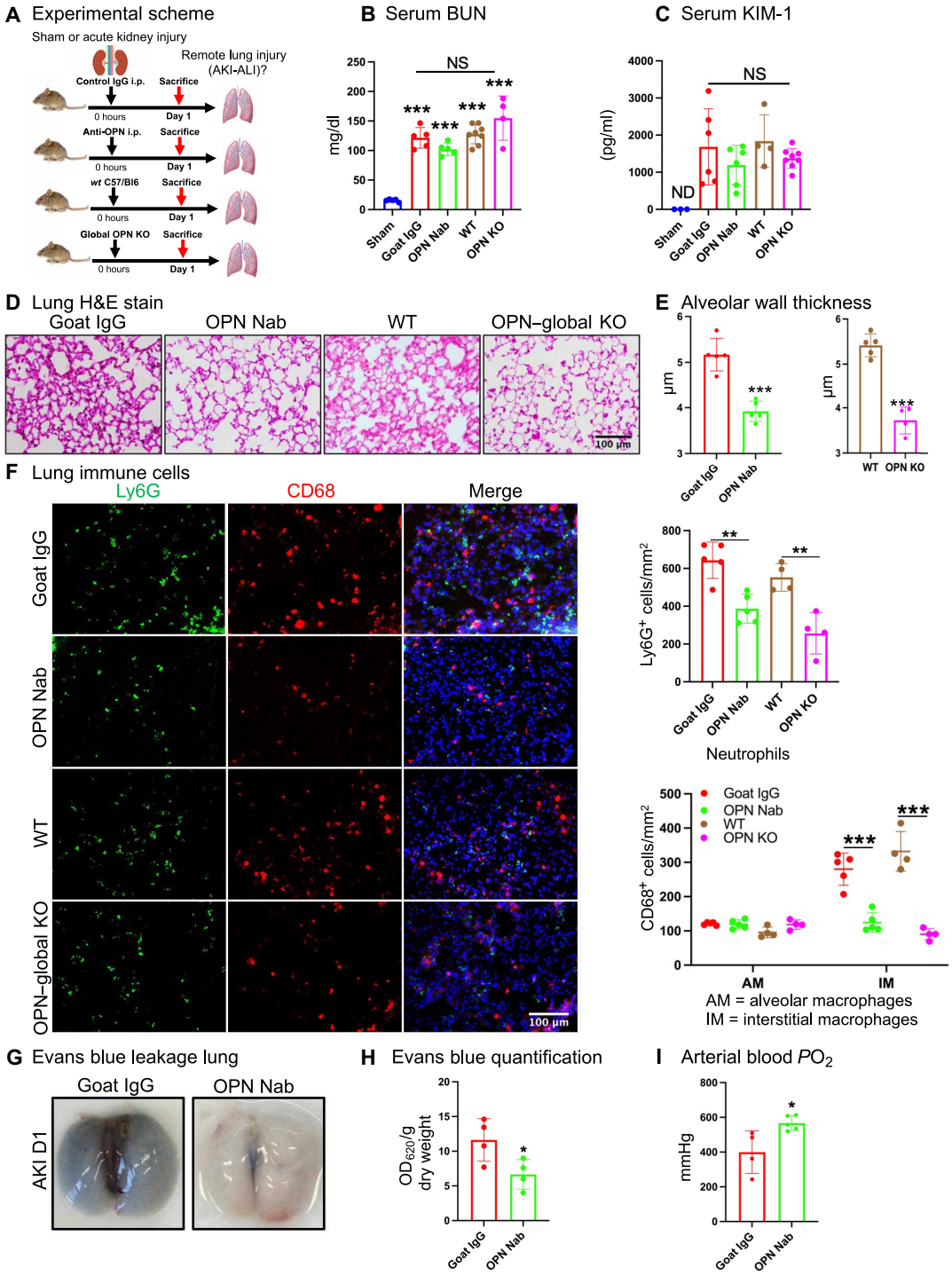

Fig. 6. Pharmacological or genetic inhibition of OPN protects from ALI after AKI. (**A**) Experimental scheme: AKI ➔ AKI-ALI model day 1 after AKI. In the following, *wt* mice injected with control goat IgG are compared to OPN neutralizing antibody (OPN Nab) injected mice, and OPN–global KO animals (OPN KO) are compared to *wt* controls. i.p., intraperitoneal. (**B**) Serum BUN values after sham or AKI, day 1. (**C**) Serum KIM-1 values after sham or AKI, day 1. (**D**) Lung hematoxylin and eosin stain after sham or AKI, day 1. (**E**) Alveolar wall thickness measurements after sham or AKI, day 1. (**F**) Lung neutrophils (Ly6G$^+$, green), alveolar macrophages (CD68^{high}, large, red), and IMs (CD68^{low}, small, red) and quantification after sham or AKI, day 1. DAPI stain (blue) was used to visualize nuclei. (**G**) Lung Evans blue leakage day 1 after sham or AKI. (**H**) Lung Evans blue quantification (OD_{620} per gram of lung dry weight) day 1 after sham or AKI. (**I**) Arterial blood oxygen partial pressure after Sham or AKI, day 1. $n = 3$ to 8 animals per measurement. *$P < 0.05$, **$P < 0.01$, and ***$P < 0.001$.

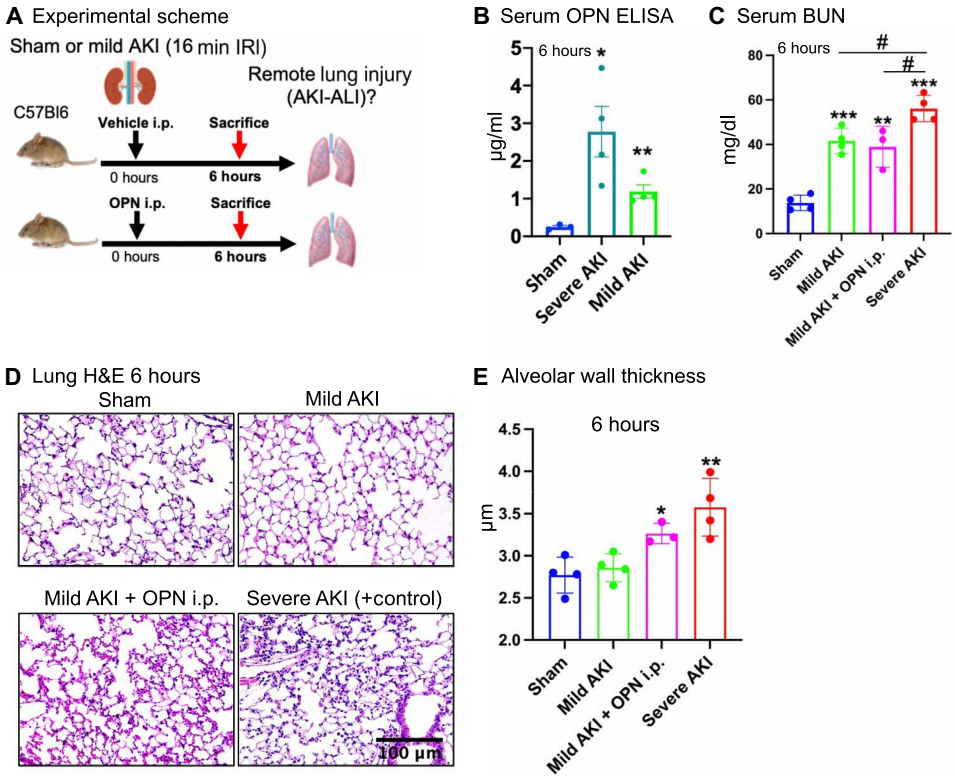

Fig. 7. Circulating OPN is sufficient to induce ALI after AKI. (**A**) Experimental scheme: AKI ➔ AKI-ALI model evaluated 6 hours after mild AKI (reduced ischemia time). Mice with mild AKI are injected with vehicle control or OPN protein, and severe AKI is used as a control. (**B**) Serum ELISA: OPN protein 6 hours after sham, severe AKI (positive control), or mild AKI. (**C**) Serum BUN 6 hours after sham, mild AKI ± OPN injection, or severe AKI (positive control). (**D**) Lung hematoxylin and eosin stain 6 hours after sham, mild AKI ± OPN injection, or severe AKI (positive control). (**E**) Alveolar wall thickness measurements 6 hours after sham, mild AKI ± OPN injection, or severe AKI (positive control). $n = 3$ to 4 animals per measurement. $^{*}P < 0.05$, $^{**}P < 0.01$, $^{***}P < 0.001$, and $\#P < 0.05$.

(see Fig. 4N). These results confirm the critical necessity for OPN in the development of AKI-ALI and suggest again that OPN may act on CD44-expressing macrophages in the lung.

DISCUSSION

Our work using kidney transplantation provides the first conclusive evidence in vivo that a kidney-released circulating mediator is causally involved in secondary organ failure after kidney injury. Neutralization of circulating OPN or OPN–global KO prevented AKI-ALI and respiratory failure, and ischemic kidneys from OPN–global KO mice transplanted into *wt* mice failed to raise serum OPN levels and to induce AKI-ALI, as compared to transplantation of ischemic *wt* kidneys into *wt* mice. In turn, transplanted *wt* kidneys reversed the protection of OPN–global KO mice against AKI-ALI, revealing the critical necessity of kidney released OPN for the development of AKI-ALI. We show that distal tubule– and proximal tubule–released OPN is poised to act as a key mediator of lung vascular leakage and inflammation early in the lung's response to kidney injury. The fast response is due to OPN's baseline expression and quick up-regulation, causing lung vascular leakage and immune cell accumulation within an hour, ultimately resulting in functional impairment with reduced arterial oxygenation. This finding has implications beyond AKI, as tissue injury due to various causes can raise OPN serum levels in humans, including but not limited to direct lung injury by COVID-19, bacterial pneumonia (*46*), sepsis from various causes (*32*, *47*, *48*), or cardiac injury (*44*, *47*). OPN has also been described as a marker of kidney injury and declining kidney function, as example (*49*, *50*), but not much is known about the mechanisms involved. All these conditions are highly associated with multiorgan failure, particularly AKI and ALI or its most severe form, ARDS. This suggests that OPN up-regulation represents a conserved response to tissue injury in different organs and might link circulating OPN to secondary organ failure in general, as it is suggested by various studies of serum OPN as a biomarker of multiorgan failure mortality in humans (*32*, *44*, *47*). Clinically, AKI-ALI is likely underrecognized because of many confounders, such as coexisting hypervolemia or cardiac dysfunction, which often serve as primary explanations for respiratory distress in patients with AKI, with AKI-induced proinflammatory contributions underestimated. In this regard, our study provides important insights. However, it is very much clinically recognized that ARDS is negatively affected by the presence of AKI (*51*) [reviewed in (*52*)]. In this context, alveolar macrophages in ARDS patients highly express OPN (*53*, *54*), and lung macrophages also express OPN in an experimental mouse model of ALI/ARDS (*53*). In addition, increased OPN levels in sputum or BAL have also been linked to inflammation and severity of disease in other human lung diseases, such as cystic fibrosis (*55*), chronic obstructive pulmonary disease (*56*), and asthma (*57*). Thus, OPN released by the AKI kidney may represent an important modifier of preexisting lung disease, particularly ALI/ARDS.

A study in mice connected OPN to lung injury after intestinal ischemia (*58*). However, in contrast to our study, OPN was found

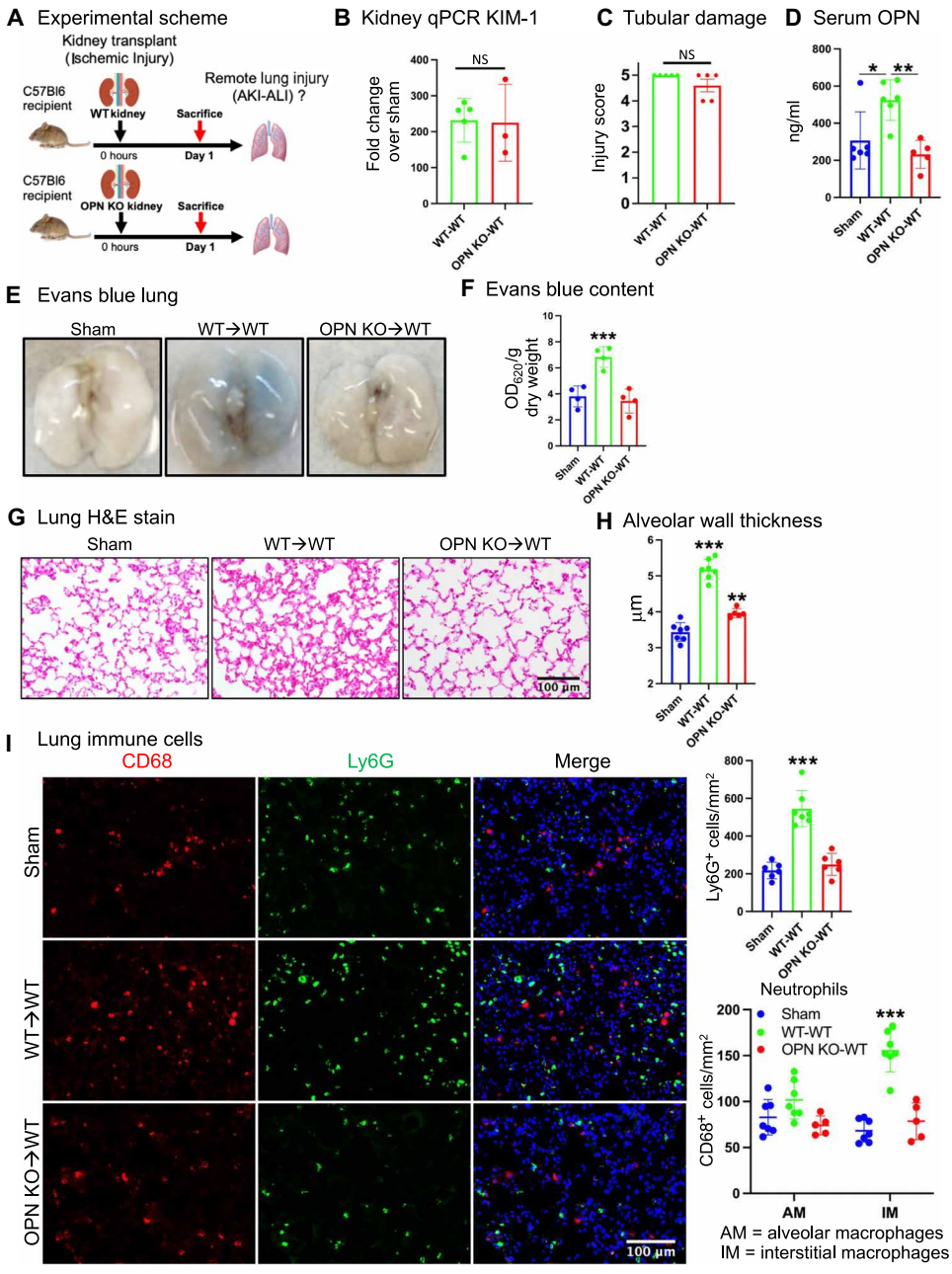

Fig. 8. Circulating OPN relevant for induction of AKI-ALI is released from the injured kidney. (**A**) Experimental scheme: Ischemic kidney transplantation. C57BL/6 *wt* or OPN–global KO kidneys were transplanted into C57BL/6 *wt* mice ("WT-WT" or "OPN KO-WT"). (**B**) Kidney qPCR: KIM-1 expression in WT-WT and OPN KO-WT day 1 after transplant. (**C**) Tubular injury score WT-WT or OPN KO-WT day 1 after transplant. (**D**) Serum ELISA: OPN protein in WT-WT and OPN KO-WT day 1 after transplant. (**E**) Lung Evans blue leakage in lungs of WT-WT and OPN KO-WT day 1 after transplant. (**F**) Lung Evans blue quantification (OD_{620} per gram of lung dry weight) in WT-WT and OPN KO-WT day 1 after transplant. (**G**) Lung hematoxylin and eosin stain of WT-WT and OPN KO-WT day 1 after transplant. (**H**) Alveolar wall thickness measurements of WT-WT and OPN KO-WT day 1 after transplant. (**I**) Lung neutrophils ($Ly6G^+$, green), alveolar macrophages ($CD68^{high}$, large, red), and IMs ($CD68^{low}$, small, red) and quantification in WT-WT and OPN KO-WT day 1 after transplant. DAPI stain (blue) was used to visualize nuclei. $n = 4$ to 7 animals per measurement. $^*P < 0.05$, $^{**}P < 0.01$, and $^{***}P < 0.001$.

up-regulated at comparably low levels in both the ischemic gut and the remotely injured lung, not allowing to identify the source of comparably low serum OPN elevations. OPN neutralization significantly improved gut injury but only mildly improved lung injury (*59*), suggesting that OPN does not represent a major causal link in gut injury–induced lung injury. A study using renal transplantation to induce ischemic AKI in rats showed that OPN is up-regulated in the lung and at rather low levels in serum at day 1 after transplantation; kidney was not assessed as an OPN source. OPN inhibition with hydrodynamic siRNA injection improved lung necroptosis and inflammation (*59*), but its effects on serum or lung OPN expression were not tested. Thus, similar to the study with intestinal ischemia, this study also did not identify OPN as a causal interorgan signal in AKI-ALI. Broadening the putative relevance of our study is the fact that remote organ effects

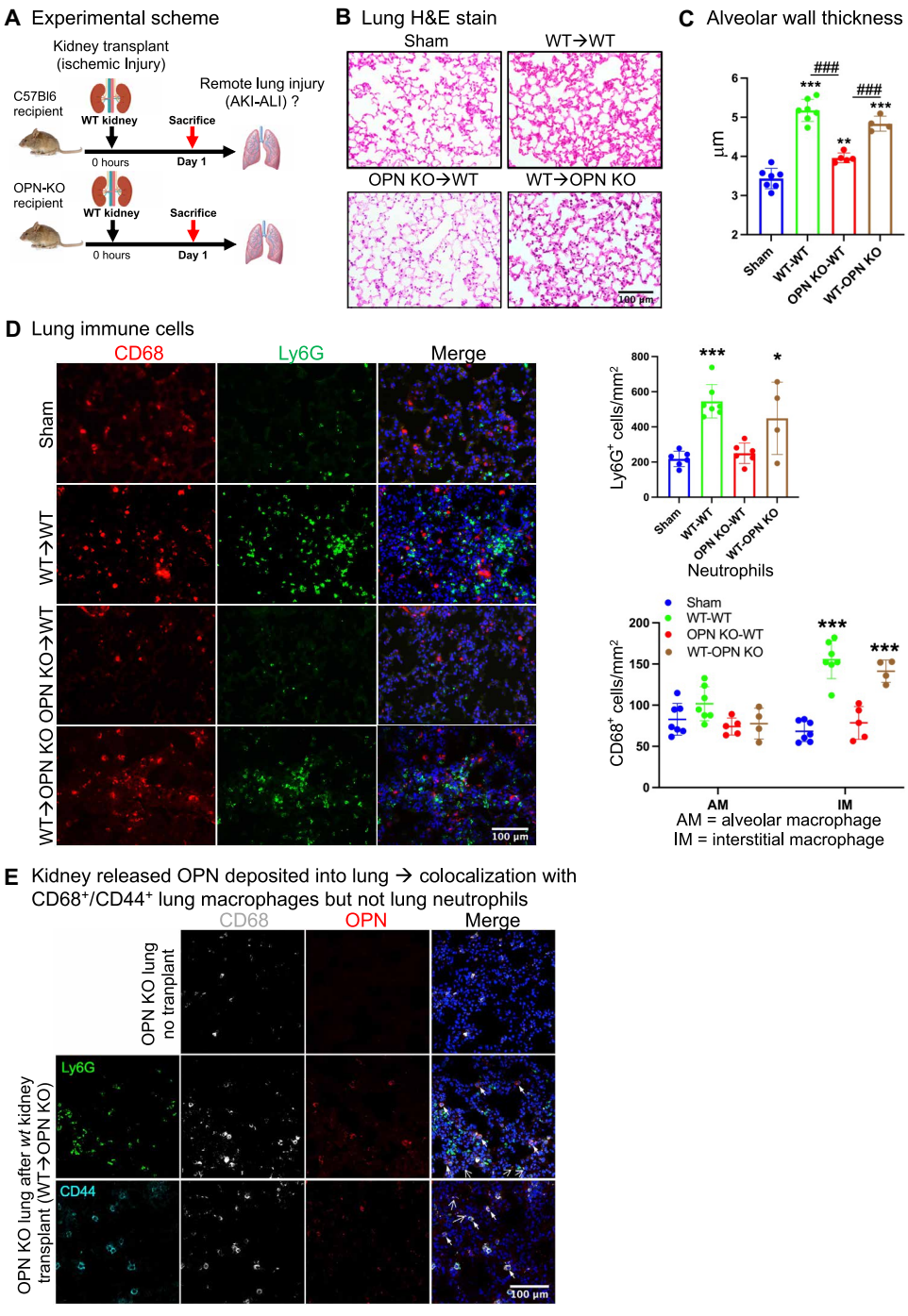

Fig. 9. Circulating OPN released from the injured kidney reverses protection of OPN-KO mice from AKI-ALI. (**A**) Experimental scheme: Ischemic kidney transplantation. *wt* kidneys were transplanted into *wt* or OPN–global KO mice (WT-WT or "WT-OPN KO"). (**B**) Lung hematoxylin and eosin stain at day 1 after transplant for WT-WT and WT-OPN KO. Sham lung and OPN KO-WT (see also Fig. 8A) are shown for comparison. (**C**) Alveolar wall thickness measurements on day 1 after transplant. (**D**) Lung neutrophils (Ly6G$^+$, green), alveolar macrophages (CD68^{high}, large, red), and IMs (CD68^{low}, small, red) and quantification in lungs of sham-operated mice, WT-WT, OPN KO-WT, or WT-OPN KO day 1 after transplant. DAPI stain (blue) was used to visualize nuclei. (**E**) Colocalization of endogenous OPN released from transplant with CD68$^+$/CD44$^+$ alveolar macrophages (fat arrows) and IMs (thin arrows) but not with Ly6G marker (neutrophils). Arrows show colocalization with CD68/CD44. $n = 4$ to 7 animals per measurement. $^*P < 0.05$, $^{**}P < 0.01$, $^{***}P < 0.001$, and $^{\#\#\#}P < 0.005$.

after AKI can also be detected in a number of other organs, including the heart and brain (*11*). OPN serum levels are elevated in the systemic inflammatory response syndrome and sepsis (*48*) and predict mortality in patients with sepsis and multiorgan failure (*31*, *32*).

One published study, which reported as primary outcome that persistently elevated OPN serum levels correlate with increased mortality in multiorgan failure patients, also suggested in secondary analysis that OPN serum levels are correlated to increased need of

ventilation (*47*), but proof of this would require new clinical trials designed to detect effects of serum OPN neutralization on respiratory outcomes. A study of critically ill patients with multiorgan failure including AKI requiring dialysis found that OPN levels in this cohort were significantly elevated when compared with critically ill controls without AKI (*44*), possibly indicating that the degree of kidney injury correlates with the degree of serum OPN elevation. Our results show that serum OPN is elevated in cases of human AKI (no multiorgan failure or sepsis) and correlates with the degree of kidney injury, strengthening the link between elevated OPN serum levels and kidney injury in humans. Together, published data and our results suggest that circulating OPN might have similar roles in AKI-ALI with respiratory failure in humans as we detect in mice.

Our studies also identify circulating OPN as a key regulator of endothelial barrier permeability in vivo in AKI-ALI. Disruption of the lung endothelial barrier and/or the pulmonary epithelial barrier is a common feature of ALI/ARDS (*34*). A number of other studies have also reported lung vascular leakage after AKI [e.g., (*18*, *37*, *60*)] and lung endothelial cell activation (*61*). For the AKI-ALI mediator TNF, this may be related to TNFR1-dependent lung endothelial cell apoptosis (*15*). However, while IL6 and TNF inhibition have been reported to strongly reduce lung neutrophil accumulation after AKI, they only moderately reduce lung vascular leakage (*15*, *37*). How IL6 and TNF relate to OPN's ability to disrupt the endothelial barrier is unknown. A previous study associated OPN with endothelial barrier permeability in pulmonary vein endothelial cells (PUVECs) in primary culture. In this report, OPN expression was increased, and ZO-1 and Cldn5 expression levels were decreased in PUVECs in septic rats or in lipopolysaccharide-treated PUVECs isolated from these rats. Up-regulation of connexin43 in PUVECs stimulated OPN expression and down-regulated ZO-1 and Cldn5, increasing vascular permeability. OPN knockdown blocked this effect (*62*, *63*). These data are consistent with our findings of ZO-1 and Cldn5 down-regulation in single-cell expression data of lung endothelial cells (Fig. 5G) and down-regulation of ZO-1 protein in immunofluorescence stains of AKI-ALI lung tissue (Fig. 5H). In addition, principally consistent with our findings, OPN was found up-regulated by the host and tumor in a mouse model of malignant pleural effusions where OPN neutralization reduced leakage of fluid into the pleural space (*64*, *65*).

TNF and its family member lymphotoxin A were also found in our L-R pairing analysis, adding additional validity to our strategy and findings. Circulating TNF is thought to participate in the induction of lung endothelial cell death via its receptor TNFR1, as neutralization of TNF with etanercept in AKI-injured *wt* mice or use of global TNFR1 KO mice reduced lung cell apoptosis after AKI (*15*). We identified various moderate to low significance pairings of TNF with its cognate receptors, particularly TNF:TNFR1, and other known interacting proteins (fig. S2). These TNF pairings were primarily identified between kidney immune cells and lung stromal or immune cells when pairing sham kidney with sham lung or at somewhat higher significance when pairing early AKI kidney (4 and 12 hours) with day 1 AKI-ALI lung. However, most of these pairings lost significance when day 1 AKI kidney was paired with day 1 AKI-ALI lung (Fig. 3, D and E, panels 1 and 2, and fig. S2). This suggests that TNF plays a role early in the development of AKI-ALI, consistent with the role of TNF as a type 1 inflammatory cytokine known to act early in establishing inflammation, and this is also consistent with the referenced study of the effect of TNF inhibition/TNFR1 deficiency on AKI-ALI (*15*). We also identified moderate to low significance L-R pairing of kidney TNF with its lung receptor TNFR2 (*Tnfrsf1b*) in immune cells but not stromal cells; however, the significance of these pairings did not increase with injury (Fig. 3, B to D, and fig. S2). Similar to TNF, IL6 was linked to AKI-ALI using IL6 neutralization and IL6 global KO mice (*16*). IL6 and its receptor, however, were not identified by our analysis.

We did not find significant lung changes after bilateral nephrectomy. Others have, however, demonstrated changes in gene expression profiles and lung inflammation after nephrectomy (*66*, *67*), and the elimination of AKI-induced cytokines can be delayed by nephrectomy (*16*). In our experiments, we can detect small changes in serum OPN even after sham surgeries, without kidney injury or nephrectomy, possibly induced by the relatively small tissue injury induced by sham surgery. It is thus possible that the detection of lung changes after nephrectomy depends, at least, in part, on the extent of tissue injury caused by the surgeon. This might explain some of the discrepancies between our work and the work of others.

OPN, also known as SPP1, early T lymphocyte activation-1, or uroprotein (*26*, *27*, *30*) is a member of the small integrin-binding ligand *N*-linked glycoprotein family proteins. OPN has, at least, two types of receptors, both broadly expressed in many cell types but highly up-regulated particularly in immune cells. It can interact with integrins via N-terminal domains and CD44 receptors via C-terminal domains. OPN interaction with CD44 causes chemotaxis of neutrophils and macrophages, whereas interactions with integrins relay immune cell spreading and activation signals (*68*–*71*). OPN (SPP1):integrin pairings were, however, not detected in our analysis. In the case of the two other predicted significant OPN (SPP1) L-R pairings, SPP1:CCR8 and SPP1:PTGER4 (prostaglandin E receptor 4) (Fig. 3B and fig. S2), it is unclear whether these interactions produce cellular signals, as these pairings were predicted by CellPhoneDB on the basis of protein-protein interaction data curated from various experimental approaches (*22*, *23*), but it is not known whether these interactions produce a cellular signal. Which target cells are affected by OPN in our model remains to be determined. In our lung scRNAseq dataset, CD44 is broadly expressed at low levels in lung stroma but robustly expressed in immune cells and highly up-regulated by injury in lung neutrophils, monocytes/macrophages, and T cells. This suggests that OPN might preferentially target immune cells rather than stromal cells of the lung.

In summary, our work identifies circulating OPN released by the injured kidney as a causal key mediator of lung endothelial leakage, lung edema, and lung inflammation with respiratory compromise. Our human sample data and available published evidence suggest that therapeutic targeting of OPN or of its associated regulatory or target components should be evaluated in patients with multiorgan failure that are at high risk of ALI or that already have ALI, particularly in the presence of AKI. Any benefit in this area could lead to a meaningful if not substantial reduction of the very high mortality of multiorgan failure.

MATERIALS AND METHODS

Animals

For all studies, adult (8 to 12 weeks old) male mice were used in accordance with the animal care and use protocol approved by the Institutional Animal Care and Use Committee of Washington University School of Medicine. C57BL/6J (B6) (JAX stock no. 000664)

and B6.129S6(Cg)-*Spp1*^{tm1Blh}/J (*OPN*$^{-/-}$) (JAX stock no. 004936) were purchased from the Jackson Laboratory.

Surgeries

Bilateral renal ischemia for 16 or 20 min (mild AKI) at 37°C was induced in both kidneys using the flank approach as previously reported by cross-clamping both renal pedicles (*72*). Sham operations were performed with exposure of both kidneys but without induction of ischemia. Syngeneic wild-type (WT) (B6 to B6) or syngeneic KO (*OPN*$^{-/-}$ to B6) kidney transplants were performed as follows: Anesthesia was induced by a mixture of ketamine (80 to 100 mg/kg) and xylazine HCl (8 to 12 mg/kg) intraperitoneally and maintained with 1 to 2% isoflurane gas, as required. Briefly, B6 or *OPN*$^{-/-}$ donor kidneys were implanted into the abdominal cavity of B6 recipient mice, where the donor suprarenal aorta and renal vein were anastomosed to the recipient infrarenal aorta and inferior vena cava, respectively. The ureter was reconstructed by direct ureter to bladder insertion (*73*). Donor kidneys were subjected to 20-min warm ischemia after procurement before they were maintained on ice for implantation, and cold ischemic times were less than 40 min. Sham-operated mice underwent the same surgical procedure except for the transplant.

Single-cell preparation for RNA sequencing

Kidneys were minced into small pieces (<1 mm^3) and incubated in tissue dissociation buffer [Liberase TM (1 mg/ml), hyaluronidase (0.7 mg/ml), and deoxyribonuclease (80 U/ml) in phosphate-buffered saline (PBS)] for 30 min in 37°C. Single cells were released from the digested tissue by pipetting 10 times, and the cell suspension was filtered through a 70-μm sieve (Falcon). Fetal bovine serum (10%) was added to stop the enzymatic reaction. Cells were collected by centrifugation (300*g* at 4°C for 5 min) and resuspended in red blood cell (RBC) lysis buffer [155 mM NH_4Cl, 10 mM $KHCO_3$, and 1 mM EDTA (pH 7.3)] for 1 min at room temperature. After washing in PBS, cells were used fresh for analysis by scRNAseq.

Single-cell RNA sequencing

scRNAseq analysis of four pooled sham or four pooled AKI samples, for both kidney and lung (sham kidney/AKI kidney and sham lung/AKI-ALI lung), was performed as described previously (*74*). Briefly, cells were stained with propidium iodide, and live cells were sorted using FACSAria III (BD Biosciences). Libraries were prepared using the Chromium Single Cell 5' Library Kit v2 and Chromium instrument (10x Genomics, Pleasanton, CA). Full-length cDNA was amplified, and libraries were submitted to Genome Technology Access Center of Washington University in St. Louis for sequencing at a depth of 50,000 reads. All processing steps were performed using Seurat v3. Quality control was first performed on each library to find appropriate filtering thresholds for each. Expression matrices for each sample were loaded into R as Seurat objects, retaining only cells that have more than 200 and less than 3200 genes. Poor quality cells with >10% mitochondrial genes were removed. Any gene not expressed in at least three cells was removed. sctransform was used for normalization scaling and variance stabilization (https://github.com/ChristophH/sctransform). This was done to reduce bias introduced by technical variation, sequencing depth, and capture efficiency. We assigned an identifier for sham kidney, AKI kidney, sham lung, and AKI-ALI lung to tell them apart. Integration of kidney and lung single-cell data was done using the harmony package (https://github.com/immunogenomics/harmony) to control for batch effects when integrating data from different samples. After quality control and integration, 13,882 kidney cells and 15,167 lung cells were further analyzed. We identified 15 clusters in the kidney and 20 clusters in the lung. We visualized cell clustering using uniform manifold approximation and projection (UMAP). To assign cluster identities, we first compiled a list of lung and kidney cell types and their currently established markers (*19*, *20*) and assessed the expression of those markers and additional known canonical markers using the FindAllMarkers() function in Seurat.

L-R pairing analysis

To infer cell-to-cell communication between kidney and lung cell types from scRNAseq or snRNAseq data, we performed L-R pairing analysis using CellPhoneDB (cellphonedb.org) (*21*). First, we integrated all datasets from kidney [sham kidney and AKI kidney (4, 12, and 24 hours)] and lung (sham lung and AKI-ALI lung) using reciprocal principal components analysis as implemented in Seurat. The 4- and 12-hour AKI kidney snRNAseq data were from published data (*19*). CellPhoneDB contains a highly curated set of human protein-protein interactions and protein complexes; thus, mouse genes were mapped to their high-confidence human one-to-one ortholog using homology mappings from Ensembl. CellPhoneDB statistical analysis was performed with default settings between all kidney and lung cell populations, conditions, and time points simultaneously to increase statistical power. Last, we considered only co-expressed pairs with a ligand expressed in a kidney cell population and its cognate receptor expressed in a lung cell population with significant cell type–specific coexpression as compared to randomly shuffled cells ($P < 0.01$). CellPhoneDB calculates an empirical P value of significance, with higher P values indicating higher significance.

Histology, immunofluorescence staining, and quantification

Mice were anesthetized by ketamine cocktail [ketamine (20 mg/ml) and xylazine (2 mg/ml) in 0.9% sodium chloride solution] and then perfused with PBS. Lungs were harvested at the indicated times. Four lobes of the right lung were cut and divided. For histology, two lobes (superior and middle lobes) were inserted into 4% paraformaldehyde, located inside a 10-ml syringe, and inflated by creating pressure with the syringe plunger after locking the syringe. After inflation, the lobes were fixed in 4% paraformaldehyde overnight at 4°C and then processed and embedded in paraffin. Sections (4 μm in thickness) were stained with hematoxylin and eosin. Alveolar wall thickness was measured as previously described using ImageJ (*75*). For immunofluorescence, one lobe (inferior lobe) of the right lung was placed into PBS, located inside a 10-ml syringe, inflated by creating pressure with the syringe plunger after locking the syringe. Fresh frozen lung sections (7 μm) were fixed in 4% paraformaldehyde, permeabilized in 0.1% Triton X-100 for 3 min, and blocked for 1 hour with 10% normal goat serum supplemented with 1% bovine serum albumin (BSA) in PBS. Sections were incubated with primary antibodies in blocking solution overnight at 4°C. The primary antibodies used were rat anti-mouse Ly6G/Ly6C (clone RB6-8C5, 14-5931, eBioscience; 1:100), rabbit anti-CD68 (ab125212, Abcam; 1:200), rat anti-mouse CD31 (550274, BD Pharmingen; 1:200), rabbit anti-ZO1 (ab221547, Abcam; 1:500), rat anti-nidogen (sc-33706, Santa Cruz Biotechnology; 1:200), rat anti-mouse CD44 (550538, BD Pharmingen; 1:200), and goat anti-mouse OPN (AF808, R&D Systems; 1:100). After extensive washes with PBS, fluorescently conjugated secondary antibodies were applied at 1:300 dilution for

1 hour at room temperature. The secondary antibodies used were as follows: Alexa Fluor 594 goat anti-rabbit (A-11037), Alexa Fluor 488 goat anti-rat (A-11006), Alexa Fluor 594 donkey anti-goat (A-11058), Alexa Fluor 647 donkey anti-rabbit (711-605-152), and Alexa Fluor 488 donkey anti-rat (712-545-153). For quantitative analysis, we selected six representative areas that were captured with a Nikon Eclipse E800 microscope at a ×200 magnification.

Electron microscopy

For transmission electron microscopy, small pieces (1- to 2-mm cubes) of lung tissue were fixed with 2% paraformaldehyde and 2% glutaraldehyde in 0.1 M sodium cacodylate buffer (pH 7.4). Embedding and sectioning were performed by the Washington University Center for Cellular Imaging. To assess the integrity of endothelial cell-cell junction, junction length was measured from digital images using ImageJ software expressed as a relation of electron dense cortical protein complex area to the total length of cell-cell contact between endothelial cells as previously described (*76*).

Evans blue injection

Mice were injected retro-orbitally with Evans blue dye (30 μg/μl; Sigma-Aldrich) in PBS (50 μg/g of body weight). After 20 min, mice were anesthetized and perfused via the left ventricle with 40 ml of PBS, and lungs were removed and additionally rinsed with PBS. The left lung was cut in half, and each half was weighed. Evans blue dye was extracted from one-half of the lung by incubation with 200 μl of formamide (56°C for 24 hours), and the concentration of Evans blue was estimated by spectrophotometer (620 nm). The other half lung was dried in an incubator set at 65°C. The dry weight was obtained after 48 hours of incubation, and the ratio of wet-to-dry weight was calculated. The resulting unit of Evans blue plasma extravasation was optical density at 620 nm (OD_{620}) per gram of dry weight (*77*).

OPN-conjugation, injection, and detection

Recombinant mouse OPN (441-OP, R&D Systems) was conjugated to Alexa Fluor 555 (A30007, Molecular Probes) according to the manufacturer. Briefly, OPN protein was reconstituted at 1 mg/ml in sterile PBS. One vial of Alexa Fluor 555 succinimidyl ester was dissolved in 10 μl of distilled H_2O. The reaction mixture containing 25 μl of recombinant OPN, 1.66 μl of Alexa Fluor 555, and 2.5 μl of 1 M sodium bicarbonate was incubated for 15 min at room temperature. After purification, the concentration of the protein was read at 280 and 555 nm using NanoDrop ND-2000C spectrophotometer (Thermo Fisher Scientific). Alexa Fluor 555–conjugated OPN was intravenously injected into mice after 20 min of bilateral renal ischemia at reperfusion or in sham mice at an equivalent matching time point. Mice were euthanized 30 min or 1 hour later, and mice were anesthetized and perfused via the left ventricle with 40 ml of PBS, before lungs were removed and additionally rinsed with PBS. Lungs were then processed to frozen sections as described and assessed for deposition of OPN into lung tissue by confocal microscopy.

Human samples

Deidentified human samples of patients with AKI without multiorgan failure, of patients with CKD or of healthy controls were provided by the Kidney Translational Research Core at Washington University in St. Louis. Cause of AKI was as follows: eight acute tubular necrosis (ATN), one oxalate crystal ATN, one AKI of obstructive etiology, one contrast nephropathy, one ureterovesical junction stone AKI, one AKI with HIV, and one AKI with malignant hypertension. Patients did not have clinical evidence of other organ failure based on clinical data review and serum biochemistries.

Quantitative reverse transcription polymerase chain reaction

Total RNA was isolated from mouse kidneys and lungs using the Direct-zol RNA MiniPrep Plus Kit (catalog no. R2072) following the manufacturers' instructions. Total RNA was reverse transcribed using the QuantiTect RT Kit (QIAGEN) and real-time polymerase chain reaction (PCR) was performed with Fast SYBR Green (QIAGEN). Primer sequences are provided in Table 1. Glyceraldehyde-3-phosphate dehydrogenase (*Gapdh*) was used as the housekeeping gene. Data were analyzed using the ΔΔCt method.

Enzyme-linked immunosorbent assay

Human OPN, mouse OPN, and mouse KIM-1 were measured in human or mouse serum samples using enzyme-linked immunosorbent assay (ELISA) kits (DY1433, DY441, and DY1817, respectively, all from R&D Systems) as per the manufacturer's instructions. Serum dilutions for ELISAs were as follows: mouse KIM-1 (1:10 dilution); mouse OPN: sham (1:2000 dilution), injured (1:4000 dilution), sham transplant (1:1000 dilution), and WT kidney transplant and OPN-KO kidney transplant (1:2000 dilution); human serum OPN: healthy control (1:500 dilution), patients with AKI (1:1000 dilution), and patients with CKD (1:500).

Mass cytometry CyTOF

Single-cell preparations were analyzed by mass cytometry as previously described (*78*). Briefly, cells were labeled using a previously validated and titrated antibody cocktail for surface markers (all antibodies conjugated by the manufacturer; Fluidigm) diluted in Fluidigm MaxPar Cell Staining Buffer (CSB) (1 hour at 4°C). After two washes in CSB, cells were fixed in 2% paraformaldehyde for 20 min at room temperature, washed, stained with MaxPar Intercalator-IR (Fluidigm), and filtered into cell strainer cap tubes. Data were then acquired on a CyTOF2/Helios instrument (Fluidigm) and analyzed with the CytoBank software using our recently described gating strategy (*78*).

Table 1. Primers.

Target gene	Primer sequence forward (5′ → 3′)	Primer sequence reverse (5′ → 3′)
Gapdh	ACCACAGTCCATGCCATCAC	TCCACCACCCTGTTGCTGTA
Havcr1 (Kim-1)	AAACCAGAGATTCCCACACG	GTCGTGGGTCTTCCTGTAGC
Spp1	GGATGAATCTGACGAATCTC	GCATCAGGATACTGTTCATC

Renal function

Serum creatinine was assessed by a liquid chromatography–mass spectrometry–based assay at the O'Brien Core Center for Acute Kidney Injury Research (University of Alabama School of Medicine, Birmingham, Alabama, USA). BUN levels were measured using the DiUR100 kit (Thermo Fisher Scientific) according to the manufacturer's instructions.

Statistical analysis

Statistical analyses were carried out using GraphPad Prism. Two-tailed, unpaired *t* tests, one-sample *t* tests, one-way analysis of variance (ANOVA), and two-way ANOVA were used to determine statistical significance in quantification. All results were expressed as means ± SD, and $P < 0.05$ was considered as statistically significant.

BAL analysis

BAL fluid was obtained by instilling saline into the lungs through a tracheal cannula using a volume equal to 80% of lung vital capacity (3× with 0.5 ml of 0.9% NaCl) for a total of 1.5 ml. Total BAL fluid recovery was approximately 90% of the instilled volume. The BAL fluid was centrifuged (400*g* for 10 min at 4°C), and the cell pellet was resuspended in PBS.

Protein and albumin concentration

Total protein concentrations in the cell-free BAL supernatant were determined using the Pierce BCA Protein Assay Kit (WJ334006, Thermo Fisher Scientific, Berkeley, MO). Albumin levels were determined with an ELISA quantification kit (W90-13, Bethyl Laboratories, Montgomery, TX) according to the manufacturers' specifications.

Flow cytometry (fluorescence-activated cell sorting) analysis of BAL cells

The cell pellet was resuspended in 0.2 ml of RBC Lysis buffer and incubated for 2 min at room temperature. Samples were blocked with Fc block (#101301, BioLegend) for 20 min before labeling for 30 min at 4°C with antibodies and washed in fluorescence-activated cell sorting (FACS) buffer (0.5% BSA, 2 mM BSA, and 0.01% NaN_3). The following antibodies, coupled to a fluorophore, were used to identify the different cell types: CD45 (#103140, BioLegend), Cd11b (#565976, BD Biosciences), Ly6G (#127627, BioLegend), CD64 (#139315, BioLegend), MERTK (MER proto-oncogene, tyrosine kinase) (#151505, BioLegend), and SiglecF (#740956, BD Biosciences). Dead cells were excluded using LIVE/DEAD Fixable Aqua stain (#L34957, Thermo Fisher Scientific). Compensation was performed at the time of sample acquisition, and flow cytometry results were analyzed using FlowJo version 10.8.1 (FlowJo LLC). All experiments were performed using BD LSRFortessa X-20. Antibody selection and manual gating strategies were defined on the basis of previous literature.

SUPPLEMENTARY MATERIALS

Supplementary material for this article is available at https://science.org/doi/10.1126/sciadv.abm5900

View/request a protocol for this paper from *Bio-protocol*.

REFERENCES AND NOTES

1. X. Zhou, R. A. Franklin, M. Adler, J. B. Jacox, W. Bailis, J. A. Shyer, R. A. Flavell, A. Mayo, U. Alon, R. Medzhitov, Circuit design features of a stable two-cell system. *Cell* **172**, 744–757.e17 (2018).
2. H. Rouault, V. Hakim, Different cell fates from cell-cell interactions: Core architectures of two-cell bistable networks. *Biophys. J.* **102**, 417–426 (2012).
3. C. Bonnans, J. Chou, Z. Werb, Remodelling the extracellular matrix in development and disease. *Nat. Rev. Mol. Cell Biol.* **15**, 786–801 (2014).
4. L. Bich, T. Pradeu, J.-F. Moreau, Understanding multicellularity: The functional organization of the intercellular space. *Front. Physiol.* **10**, 1170 (2019).
5. J. P. Teixeira, S. Ambruso, B. R. Griffin, S. Faubel, Pulmonary consequences of acute kidney injury. *Semin. Nephrol.* **39**, 3–16 (2019).
6. S. Faubel, C. L. Edelstein, Mechanisms and mediators of lung injury after acute kidney injury. *Nat. Rev. Nephrol.* **12**, 48–60 (2016).
7. M. Darmon, C. Clec'h, C. Adrie, L. Argaud, B. Allaouchiche, E. Azoulay, L. Bouadma, M. Garrouste-Orgeas, H. Haouache, C. Schwebel, D. Goldgran-Toledano, H. Khallel, A.-S. Dumenil, S. Jamali, B. Souweine, F. Zeni, Y. Cohen, J.-F. Timsit, Acute respiratory distress syndrome and risk of AKI among critically ill patients. *Clin. J. Am. Soc. Nephrol.* **9**, 1347–1353 (2014).
8. B. T. Thompson, R. C. Chambers, K. D. Liu, Acute respiratory distress syndrome. *N. Engl. J. Med.* **377**, 562–572 (2017).
9. P. Lertjitbanjong, C. Thongprayoon, W. Cheungpasitporn, O. A. O'Corragain, N. Srivali, T. Bathini, K. Watthanasuntorn, N. R. Aeddula, S. A. Salim, P. Ungprasert, E. A. Gillaspie, K. Wijarnpreecha, M. A. Mao, W. Kaewput, Acute kidney injury after lung transplantation: A systematic review and meta-analysis. *J. Clin. Med.* **8**, 1713 (2019).
10. J. Gameiro, J. A. Fonseca, C. Outerelo, J. A. Lopes, Acute kidney injury: From diagnosis to prevention and treatment strategies. *J. Clin. Med.* **9**, 1704 (2020).
11. S. A. Lee, M. Cozzi, E. L. Bush, H. Rabb, Distant organ dysfunction in acute kidney injury: A review. *Am. J. Kidney Dis.* **72**, 846–856 (2018).
12. P. Aranda-Valderrama, A. M. Kaynar, The basic science and molecular mechanisms of lung injury and acute respiratory distress syndrome. *Int. Anesthesiol. Clin.* **56**, 1–25 (2018).
13. C. L. Klein, T. S. Hoke, W.-F. Fang, C. J. Altmann, I. S. Douglas, S. Faubel, Interleukin-6 mediates lung injury following ischemic acute kidney injury or bilateral nephrectomy. *Kidney Int.* **74**, 901–909 (2008).
14. N. Ahuja, A. Andres-Hernando, C. Altmann, R. Bhargava, J. Bacalja, R. G. Webb, Z. He, C. L. Edelstein, S. Faubel, Circulating IL-6 mediates lung injury via CXCL1 production after acute kidney injury in mice. *Am. J. Physiol. Renal Physiol.* **303**, F864–F872 (2012).
15. L. E. White, R. J. Santora, Y. Cui, F. A. Moore, H. T. Hassoun, TNFR1-dependent pulmonary apoptosis during ischemic acute kidney injury. *Am. J. Physiol. Lung Cell. Mol. Physiol.* **303**, L449–L459 (2012).
16. A. A. Hernando, K. Okamura, R. Bhargava, C. M. Kiekhaefer, D. Soranno, L. A. Kirkbride-Romeo, H.-W. Gil, C. Altmann, S. Faubel, Circulating IL-6 upregulates IL-10 production in splenic CD4+ T cells and limits acute kidney injury-induced lung inflammation. *Kidney Int.* **91**, 1057–1069 (2017).
17. L. E. White, Y. Cui, C. M. F. Shelak, M. L. Lie, H. T. Hassoun, Lung endothelial cell apoptosis during ischemic acute kidney injury. *Shock* **38**, 320–327 (2012).
18. F. F. Hoyer, K. Naxerova, M. J. Schloss, M. Hulsmans, A. V. Nair, P. Dutta, D. M. Calcagno, F. Herisson, A. Anzai, Y. Sun, G. Wojtkiewicz, D. Rohde, V. Frodermann, K. Vandoorne, G. Courties, Y. Iwamoto, C. S. Garris, D. L. Williams, S. Breton, D. Brown, M. Whalen, P. Libby, M. J. Pittet, K. R. King, R. Weissleder, F. K. Swirski, M. Nahrendorf, Tissue-specific macrophage responses to remote injury impact the outcome of subsequent local immune challenge. *Immunity* **51**, 899–914.e7 (2019).
19. Y. Kirita, H. Wu, K. Uchimura, P. C. Wilson, B. D. Humphreys, Cell profiling of mouse acute kidney injury reveals conserved cellular responses to injury. *Proc. Natl. Acad. Sci. U.S.A.* **117**, 15874–15883 (2020).
20. I. Angelidis, L. M. Simon, I. E. Fernandez, M. Strunz, C. H. Mayr, F. R. Greiffo, G. Tsitsiridis, M. Ansari, E. Graf, T.-M. Strom, M. Nagendran, T. Desai, O. Eickelberg, M. Mann, F. J. Theis, H. B. Schiller, An atlas of the aging lung mapped by single cell transcriptomics and deep tissue proteomics. *Nat. Commun.* **10**, 963 (2019).
21. M. Efremova, M. Vento-Tormo, S. A. Teichmann, R. Vento-Tormo, CellPhoneDB: Inferring cell–cell communication from combined expression of multi-subunit ligand–receptor complexes. *Nat. Protoc.* **15**, 1484–1506 (2020).
22. K. R. Brown, I. Jurisica, Unequal evolutionary conservation of human protein interactions in interologous networks. *Genome Biol.* **8**, R95 (2007).
23. K. R. Brown, I. Jurisica, Online predicted human interaction database. *Bioinformatics* **21**, 2076–2082 (2005).
24. T. E. Kruger, A. H. Miller, A. K. Godwin, J. Wang, Bone sialoprotein and osteopontin in bone metastasis of osteotropic cancers. *Crit. Rev. Oncol. Hematol.* **89**, 330–341 (2014).
25. S. K. Ramaiah, S. Rittling, Pathophysiological role of osteopontin in hepatic inflammation, toxicity, and cancer. *Toxicol. Sci.* **103**, 4–13 (2008).
26. L. W. Fisher, D. A. Torchia, B. Fohr, M. F. Young, N. S. Fedarko, Flexible structures of SIBLING proteins, bone sialoprotein, and osteopontin. *Biochem. Biophys. Res. Commun.* **280**, 460–465 (2001).
27. R. Pichler, C. M. Giachelli, D. Lombardi, J. Pippin, K. Gordon, C. E. Alpers, S. M. Schwartz, R. J. Johnson, Tubulointerstitial disease in glomerulonephritis. Potential role of osteopontin (uropontin). *Am. J. Pathol.* **144**, 915–926 (1994).
28. A. Oldberg, A. Franzén, D. Heinegård, Cloning and sequence analysis of rat bone sialoprotein (osteopontin) cDNA reveals an Arg-Gly-Asp cell-binding sequence. *Proc. Natl. Acad. Sci. U.S.A.* **83**, 8819–8823 (1986).

29. D. T. Denhardt, X. Guo, Osteopontin: A protein with diverse functions. *FASEB J.* **7**, 1475–1482 (1993).
30. S. Ashkar, G. F. Weber, V. Panoutsakopoulou, M. E. Sanchirico, M. Jansson, S. Zawaideh, S. R. Rittling, D. T. Denhardt, M. J. Glimcher, H. Cantor, Eta-1 (osteopontin): An early component of type-1 (cell-mediated) immunity. *Science* **287**, 860–864 (2000).
31. L. M. Castello, M. Baldrighi, L. Molinari, L. Salmi, V. Cantaluppi, R. Vaschetto, G. Zunino, M. Quaglia, M. Bellan, F. Gavelli, P. Navalesi, G. C. Avanzi, A. Chiocchetti, The role of osteopontin as a diagnostic and prognostic biomarker in sepsis and septic shock. *Cell* **8**, 174 (2019).
32. F. Carbone, A. Bonaventura, A. Vecchiè, J. Meessen, S. Minetti, E. Elia, D. Ferrara, A. M. Ansaldo, G. Tulli, D. Guarducci, N. Rossi, F. Bona, M. Ferrari, P. Caironi, R. Latini, F. Montecucco, Early osteopontin levels predict mortality in patients with septic shock. *Eur. J. Intern. Med.* **78**, 113–120 (2020).
33. A. G. Vassiliou, A. Kotanidou, I. Dimopoulou, S. E. Orfanos, Endothelial damage in acute respiratory distress syndrome. *Int. J. Mol. Sci.* **21**, 8793 (2020).
34. E. V. Dolmatova, K. Wang, R. Mandavilli, K. K. Griendling, The effects of sepsis on endothelium and clinical implications. *Cardiovasc. Res.* **117**, 60–73 (2021).
35. R. S. Hotchkiss, L. L. Moldawer, S. M. Opal, K. Reinhart, I. R. Turnbull, J.-L. Vincent, Sepsis and septic shock. *Nat. Rev. Dis. Primers.* **2**, 16045 (2016).
36. L. Michalick, S. Weidenfeld, B. Grimmer, D. Fatykhova, P. D. Solymosi, F. Behrens, M. Dohmen, M. C. Brack, S. Schulz, E. Thomasch, S. Simmons, H. Müller-Redetzky, N. Suttorp, F. Kurth, J. Neudecker, M. Toennies, T. T. Bauer, S. Eggeling, V. M. Corman, A. C. Hocke, M. Witzenrath, S. Hippenstiel, W. M. Kuebler, Plasma mediators in patients with severe COVID-19 cause lung endothelial barrier failure. *Eur. Respir. J.* **57**, 2002384 (2021).
37. C. L. Klein, T. S. Hoke, W.-F. Fang, C. J. Altmann, I. S. Douglas, S. Faubel, Interleukin-6 mediates lung injury following ischemic acute kidney injury or bilateral nephrectomy. *Kidney Int.* **74**, 901–909 (2008).
38. A. A. Kramer, G. Postler, K. F. Salhab, C. Mendez, L. C. Carey, H. Rabb, Renal ischemia/reperfusion leads to macrophage-mediated increase in pulmonary vascular permeability. *Kidney Int.* **55**, 2362–2367 (1999).
39. S. Ministrini, F. Carbone, F. Montecucco, Emerging role for the inflammatory biomarker osteopontin in adverse cardiac remodeling. *Biomark. Med.* **14**, 1303–1306 (2020).
40. S. R. Martinez, D. I. Fernández, V. M. M. Cuesta, F. Genre, V. Pulito-Cueto, S. M. F. Rozas, L. Lera-Gómez, B. Atienza-Mateo, R. López-Mejías, M. A. González-Gay, J. M. Cifrián, Osteopontin and interleukin-6 as biomarkers of interstitial lung disease. *Eur. Respir. J* **56**, 2717 (2020).
41. C. Varım, T. Demirci, H. Cengiz, İ. Hacıbekiroğlu, F. B. Tuncer, E. Çokluk, H. Toptan, O. Karabay, İ. Yıldırım, Relationship between serum osteopontin levels and the severity of COVID-19 infection. *Wien. Klin. Wochenschr.* **133**, 298–302 (2021).
42. S. H. Loosen, C. Roderburg, K. L. Kauertz, I. Pombeiro, C. Leyh, F. Benz, M. Vucur, T. Longerich, A. Koch, T. Braunschweig, T. F. Ulmer, C. Heidenhain, F. Tacke, M. Binnebösel, M. Schmeding, C. Trautwein, U. P. Neumann, T. Luedde, Elevated levels of circulating osteopontin are associated with a poor survival after resection of cholangiocarcinoma. *J. Hepatol.* **67**, 749–757 (2017).
42. M. Behnes, M. Brueckmann, S. Lang, F. Espeter, C. Weiss, M. Neumaier, P. Ahmad-Nejad, M. Borggrefe, U. Hoffmann, Diagnostic and prognostic value of osteopontin in patients with acute congestive heart failure. *Eur. J. Heart Fail.* **15**, 1390–1400 (2013).
44. J. M. Lorenzen, C. Hafer, R. Faulhaber-Walter, P. Kümpers, J. T. Kielstein, H. Haller, D. Fliser, Osteopontin predicts survival in critically ill patients with acute kidney injury. *Nephrol. Dial. Transplant.* **26**, 531–537 (2010).
45. M. Rosenberg, C. Zugck, M. Nelles, C. Juenger, D. Frank, A. Remppis, E. Giannitsis, H. A. Katus, N. Frey, Osteopontin, a new prognostic biomarker in patients with chronic heart failure. *Circ. Heart Fail.* **1**, 43–49 (2008).
46. G. Cappellano, H. Abreu, D. Raineri, L. Scotti, L. Castello, R. Vaschetto, A. Chiocchetti, High levels of circulating osteopontin in inflammatory lung disease regardless of Sars-CoV-2 infection. *EMBO Mol. Med.* **13**, e14124 (2021).
47. C. Roderburg, F. Benz, D. V. Cardenas, M. Lutz, H.-J. Hippe, T. Luedde, C. Trautwein, N. Frey, A. Koch, F. Tacke, M. Luedde, Persistently elevated osteopontin serum levels predict mortality in critically ill patients. *Crit. Care* **19**, 271 (2015).
48. R. Vaschetto, S. Nicola, C. Olivieri, E. Boggio, F. Piccolella, R. Mesturini, F. Damnotti, D. Colombo, P. Navalesi, F. D. Corte, U. Dianzani, A. Chiocchetti, Serum levels of osteopontin are increased in SIRS and sepsis. *Intensive Care Med.* **34**, 2176–2184 (2008).
49. E. Owens, K.-S. Tan, R. Ellis, S. D. Vecchio, T. Humphries, E. Lennan, D. Vesey, H. Healy, W. Hoy, G. Gobe, Development of a biomarker panel to distinguish risk of progressive chronic kidney disease. *Biomedicine* **8**, 606 (2020).
50. Z.-K. Jin, P.-X. Tian, X.-Z. Wang, W.-J. Xue, X.-M. Ding, J. Zheng, C.-G. Ding, T.-C. Mao, W.-L. Duan, M. Xi, Kidney injury molecule-1 and osteopontin: New markers for prediction of early kidney transplant rejection. *Mol. Immunol.* **54**, 457–464 (2013).
51. K. D. Liu, D. V. Glidden, M. D. Eisner, P. E. Parsons, L. B. Ware, A. Wheeler, A. Korpak, T. B. Thompson, G. M. Chertow, M. A. Matthay; National Heart, Lung, and Blood Institute ARDS Network Clinical Trials Group, Predictive and pathogenetic value of plasma biomarkers for acute kidney injury in patients with acute lung injury. *Crit. Care Med.* **35**, 2755–2761 (2007).
52. J. Alge, K. Dolan, J. Angelo, S. Thadani, M. Virk, A. A. Arikan, Two to tango: Kidney-lung interaction in acute kidney injury and acute respiratory distress syndrome. *Front. Pediatr.* **9**, 744110 (2021).
53. F. Takahashi, K. Takahashi, K. Shimizu, R. Cui, N. Tada, H. Takahashi, S. Soma, M. Yoshioka, Y. Fukuchi, Osteopontin is strongly expressed by alveolar macrophages in the lungs of acute respiratory distress syndrome. *Lung* **182**, 173–185 (2004).
54. G. Kasetty, P. Papareddy, R. K. V. Bhongir, M. N. Ali, M. Mori, M. Wygrecka, J. S. Erjefält, A. Hultgårdh-Nilsson, L. Palmberg, H. Herwald, A. Egesten, Osteopontin protects against lung injury caused by extracellular histones. *Mucosal Immunol.* **12**, 39–50 (2019).
55. S. Jovic, M. Shikhagaie, M. Mörgelin, J. S. Erjefält, S. Kjellström, A. Egesten, Osteopontin is increased in cystic fibrosis and can skew the functional balance between ELR-positive and ELR-negative CXC-chemokines. *J. Cyst. Fibros.* **14**, 453–463 (2015).
56. A. Papaporfyriou, S. Loukides, K. Kostikas, D. C. M. Simoes, G. Papatheodorou, E. Konstantellou, G. Hillas, S. Papiris, N. Koulouris, P. Bakakos, Increased levels of osteopontin in sputum supernatant in patients with COPD. *Chest* **146**, 951–958 (2014).
57. K. Samitas, E. Zervas, S. Vittorakis, M. Semitekolou, T. Alissafi, A. Bossios, H. Gogos, E. Economidou, J. Lotvall, G. Xanthou, V. Panoutsakopoulou, M. Gaga, Osteopontin expression and relation to disease severity in human asthma. *Eur. Respir. J.* **37**, 331–341 (2010).
58. Y. Hirano, M. Aziz, W.-L. Yang, M. Ochani, P. Wang, Neutralization of osteopontin ameliorates acute lung injury induced by intestinal ischemia-reperfusion. *Shock* **46**, 431–438 (2016).
59. H. Zhao, Q. Chen, H. Huang, K. C. Suen, A. Alam, J. Cui, S. Ciechanowicz, J. Ning, K. Lu, M. Takata, J. Gu, D. Ma, Osteopontin mediates necroptosis in lung injury after transplantation of ischaemic renal allografts in rats. *Br. J. Anaesth.* **123**, 519–530 (2019).
60. H. T. Hassoun, M. L. Lie, D. N. Grigoryev, M. Liu, R. M. Tuder, H. Rabb, Kidney ischemia-reperfusion injury induces caspase-dependent pulmonary apoptosis. *Am. J. Physiol. Renal Physiol.* **297**, F125–F137 (2009).
61. C. M. Feltes, H. T. Hassoun, M. L. Lie, C. Cheadle, H. Rabb, Pulmonary endothelial cell activation during experimental acute kidney injury. *Shock* **36**, 170–176 (2011).
62. J. Zhang, G. Yang, Y. Zhu, X. Peng, T. Li, L. Liu, Relationship of Cx43 regulation of vascular permeability to osteopontin-tight junction protein pathway after sepsis in rats. *Am. J. Physiol. Regul. Integr. Comp. Physiol.* **314**, R1–R11 (2017).
63. J. Zhang, G.-M. Yang, Y. Zhu, X.-Y. Peng, T. Li, L.-M. Liu, Role of connexin 43 in vascular hyperpermeability and relationship to Rock1-MLC20 pathway in septic rats. *Am. J. Physiol. Lung Cell. Mol. Physiol.* **309**, L1323–L1332 (2015).
64. C. Moschos, I. Porfiridis, I. Psallidas, A. Kollintza, G. T. Stathopoulos, S. A. Papiris, C. Roussos, I. Kalomenidis, Osteopontin is upregulated in malignant and inflammatory pleural effusions. *Respirology* **14**, 716–722 (2009).
65. I. Psallidas, G. T. Stathopoulos, N. A. Maniatis, S. Magkouta, C. Moschos, S. P. Karabela, A. Kollintza, D. C. M. Simoes, M. Kardara, S. Vassiliou, S. A. Papiris, C. Roussos, I. Kalomenidis, Secreted phosphoprotein-1 directly provokes vascular leakage to foster malignant pleural effusion. *Oncogene* **32**, 528–535 (2013).
66. H. T. Hassoun, D. N. Grigoryev, M. L. Lie, M. Liu, C. Cheadle, R. M. Tuder, H. Rabb, Ischemic acute kidney injury induces a distant organ functional and genomic response distinguishable from bilateral nephrectomy. *Am. J. Physiol. Renal Physiol.* **293**, F30–F40 (2007).
67. T. S. Hoke, I. S. Douglas, C. L. Klein, Z. He, W. Fang, J. M. Thurman, Y. Tao, B. Dursun, N. F. Voelkel, C. L. Edelstein, S. Faubel, Acute renal failure after bilateral nephrectomy is associated with cytokine-mediated pulmonary injury. *J. Am. Soc. Nephrol.* **18**, 155–164 (2007).
68. B. Zhu, K. Suzuki, H. A. Goldberg, S. R. Rittling, D. T. Denhardt, C. A. G. McCulloch, J. Sodek, Osteopontin modulates CD44-dependent chemotaxis of peritoneal macrophages through G-protein-coupled receptors: Evidence of a role for an intracellular form of osteopontin. *J. Cell. Physiol.* **198**, 155–167 (2004).
69. A. Koh, A. P. B. D. Silva, A. K. Bansal, M. Bansal, C. Sun, H. Lee, M. Glogauer, J. Sodek, R. Zohar, Role of osteopontin in neutrophil function. *Immunology* **122**, 466–475 (2007).
70. Y. Hirano, M. Aziz, W.-L. Yang, Z. Wang, M. Zhou, M. Ochani, A. Khader, P. Wang, Neutralization of osteopontin attenuates neutrophil migration in sepsis-induced acute lung injury. *Crit. Care* **19**, 53 (2015).
71. H. R. Moorman, D. Poschel, J. D. Klement, C. Lu, P. S. Redd, K. Liu, Osteopontin: A key regulator of tumor progression and immunomodulation. *Cancer* **12**, 3379 (2020).
72. L. Yang, T. Y. Besschetnova, C. R. Brooks, J. V. Shah, J. V. Bonventre, Epithelial cell cycle arrest in G2/M mediates kidney fibrosis after injury. *Nat. Med.* **16**, 535–543 (2010).
73. W. R. Han, L. J. Murray-Segal, P. L. Mottram, Modified technique for kidney transplantation in mice. *Microsurgery* **19**, 272–274 (1999).
74. J. W. Williams, H. Winkels, C. P. Durant, K. Zaitsev, Y. Ghosheh, K. Ley, Single cell RNA sequencing in atherosclerosis research. *Circ. Res.* **126**, 1112–1126 (2020).

75. Z. J. Pua, B. S. Stonestreet, A. Cullen, A. Shahsafaei, G. B. Sadowska, M. E. Sunday, Histochemical analyses of altered fetal lung development following single vs multiple courses of antenatal steroids. *J. Histochem. Cytochem.* **53**, 1469–1479 (2005).
76. L. Hakanpaa, E. A. Kiss, G. Jacquemet, I. Miinalainen, M. Lerche, C. Guzmán, E. Mervaala, L. Eklund, J. Ivaska, P. Saharinen, Targeting β1-integrin inhibits vascular leakage in endotoxemia. *Proc. Natl. Acad. Sci. U.S.A.* **115**, E6467–E6476 (2018).
77. M. J. Wick, J. W. Harral, Z. L. Loomis, E. C. Dempsey, An optimized Evans blue protocol to assess vascular leak in the mouse. *J. Vis. Exp.* , 57037 (2018).
78. S. L. Brody, S. P. Gunsten, H. P. Luehmann, D. H. Sultan, M. Hoelscher, G. S. Heo, J. Pan, J. R. Koenitzer, E. C. Lee, T. Huang, C. Mpoy, S. Guo, R. Laforest, A. Salter, T. D. Russell, A. Shifren, C. Combadiere, K. J. Lavine, D. Kreisel, B. D. Humphreys, B. E. Rogers, D. S. Gierada, D. E. Byers, R. J. Gropler, D. L. Chen, J. J. Atkinson, Y. Liu, Chemokine receptor 2–targeted molecular imaging in pulmonary fibrosis. A clinical trial. *Am. J. Resp. Crit. Care Med.* **203**, 78–89 (2021).

Acknowledgments: We are grateful to S. Jain, M. Rauchman, and P. Herrlich for numerous discussions, insights, and reviewing this manuscript. We also thank K. Conlon and the Kidney Translational Research Center at Washington University (supported by the Division of Nephrology and P30 DK079333) for providing clinical data and samples from patients with AKI. **Funding:** A.H. and this work were supported by NIH RO1s DK121200, DK108947, and VA Merit Award BX005322, and E.K. was supported by the American Heart Association Career Development Award 20CDA35320006 and the American Society of Nephrology Career Development Award (KidneyCure Carl W. Gottschalk Research Scholar Grant). **Author contributions:** F.Z.K. performed the scRNAseq analysis, contributed to tissue analysis, performed FACS experiments, and designed figures. L.N. performed animal surgeries, most of the tissue analysis, BAL acquisition, and protein assays and designed figures. E.K. performed animal surgeries and mass cytometry (CyTOF) experiments, supervised experiments and data analysis, and helped with manuscript writing and editing. H.D. performed kidney transplants. A.A. performed mouse OPN and KIM-1 ELISAs, as well as part of the OPN qPCR measurements. A.K. performed human OPN ELISAs and part of the OPN qPCR measurements. J.J.A. provided reagents and expertise for CyTOF experiments and their analysis. W.L. performed mouse intubations and blood gas measurements. B.W. supervised kidney transplants. S.D. carried out the CellPhoneDB analysis and provided help with the scRNAseq analysis. K.L. helped with design, technical aspects, and analysis of scRNAseq experiments and participated in manuscript writing and editing. D.K. provided expertise for analysis of the lung phenotype, supervised mouse intubations and blood gas measurements, helped supervise transplant experiments, and participated in manuscript writing and editing. A.H. conceived the idea for the project, designed all experiments (with select input by K.L., D.K., and B.W.), supervised their analysis, and wrote the manuscript. **Competing interests:** A.H. has filed a patent application (pending) related to this work. The other authors declare that they have no competing interests. **Data and materials availability:** All data needed to evaluate the conclusions in the paper are present in the paper and/or the Supplementary Materials.

Submitted 28 September 2021
Accepted 30 December 2021
Published 25 February 2022
10.1126/sciadv.abm5900

ScienceAdvances

Identification of kidney injury–released circulating osteopontin as causal agent of respiratory failure

Fatima Zohra KhamissiLiang NingEirini KefaloyianniHao DunAkshayakeerthi ArthanarisamiAmy KellerJeffrey J. AtkinsonWenjun LiBrian WongSabine DietmannKory LavineDaniel KreiselAndreas Herrlich

Sci. Adv., 8 (8), eabm5900. • DOI: 10.1126/sciadv.abm5900

Science Advances (ISSN) is published by the American Association for the Advancement of Science. 1200 New York Avenue NW, Washington, DC 20005. The title *Science Advances* is a registered trademark of AAAS.